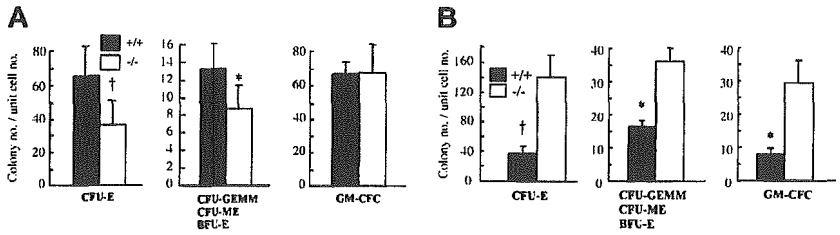

Figure 3. Colony-forming activity of hematopoietic progenitor cells from OSMR$^{+/+}$ and OSMR$^{-/-}$ mice. CFU-Es (A,D), CFU-GEMMs/CFU-MEs/BFU-Es (B,E), and GM-CFCs (C,F) from hematopoietic cells of OSMR$^{+/+}$ and OSMR$^{-/-}$ mice are shown. The figure shows mean total colony number ± SD (n = 5 to 7) in triplicate cultures containing 25 000 BM cells (A-C) or 100 000 spleen cells (D-F) stimulated with final concentrations of IL-3 at 10 ng/mL, SCF at 80 ng/mL, and EPO at 4 U/mL. *$P < .05$ between wild-type and mutant mice. †$P < .01$ between wild-type and mutant mice.

(Figure 3B). In contrast, there was no difference in granulocyte-macrophage colony-forming cells (GM-CFCs) including granulocyte CFUs (CFU-Gs), macrophage CFUs (CFU-Ms), and granulocyte-macrophage CFUs (CFU-GMs) (Figure 3C). These results are consistent with the peripheral blood cells in mutant mice.

It is known that the spleen is a second hematopoietic organ and becomes a major site for murine erythropoiesis under conditions that severely damage erythrocytes.[41] Since OSMR is expressed in spleen at a relatively high level, we examined hematopoietic progenitors in mutant and wild-type spleen by in vitro clonal cultures. In contrast to BM, the number of CFU-Es in mutant spleen was markedly increased compared with wild-type control (Figure 3D). In addition, the numbers of all types of colonies including CFU-GEMMs, CFU-MEs, BFU-Es, and GM-CFCs were also maintained at higher levels (Figure 3E-F). These results suggested that OSM might have an opposite effect on hematopoiesis in BM and spleen.

Recovery of erythrocytes from chemically induced acute hemolysis

The mutant mice displayed a slightly anemic phenotype and a reduced reservoir of erythrocyte precursors in marrow. To investigate whether OSM itself affects erythropoiesis or not, we assessed wild-type and mutant erythropoiesis in response to acute hemolysis induced by phenylhydrazine (PHZ). We injected PHZ into mutant and wild-type mice intraperitoneally on days 0 and 1. The recovery was monitored by measurement of peripheral red cells, reticulocytes, and CFU-Es in marrow and spleen. The recovery of peripheral red cells as measured by hematocrit was similar in both genotypes (Figure 4A). Reticulocytes are newly generated red blood cells and become mature red cells within 2 days. After administration of PHZ, the number of reticulocytes in wild-type and mutant mice increased sharply with similar kinetics (Figure 4B). Analysis of erythroid progenitor CFU-Es revealed that there was no difference in the initial rate of increase between wild-type and mutant marrow (Figure 4C). Although the number of CFU-Es in mutant spleen was higher than that of wild-type spleen, the rate of increase was not so different, indicating that CFU-E numbers in spleen after PHZ administration reflected the original ratio of CFU-Es between wild-type and mutant mice (Figure 4D). These results strongly suggested that erythroid progenitors in OSMR-deficient mice are capable of responding to acute hemolysis and of differentiating to mature erythrocytes normally.

Since 5-FU selectively kills cycling cells and results in myelosuppression,[42] the recovery from such stress needs proliferation and differentiation of dormant stem cells. To assess the recovery of hematopoiesis in BM, we intravenously injected 5-FU into mutant and wild-type mice. The BM progenitors in a femur were examined at 2, 5, and 8 days after 5-FU administration. The kinetics of recovery of BM progenitors in OSMR$^{-/-}$ mice paralleled those of OSMR$^{+/+}$ mice (data not shown). These results suggested that BM progenitor cells of OSMR$^{-/-}$ mice are able to respond to acute hemolysis and myelosuppression normally.

Analysis of megakaryocyte progenitors

Analysis of peripheral blood cells demonstrated that the platelets as well as erythrocytes were reduced in OSMR$^{-/-}$ mice. Megakaryopoiesis is a regulated process by which multipotential hematopoietic cells commit to megakaryocytes that release platelets after several maturation steps.[43,44] Therefore, the number of peripheral platelets depends on the number and maturation process of megakaryocyte progenitors. To determine which stage of platelet production is affected by the lack of OSM function, we examined the number of megakaryocytes in mutant and wild-type BM. The number of megakaryocytes in mutant BM was significantly reduced compared with control (Figure 5A). To compare the numbers of megakaryocyte progenitors in mutant and wild-type BM, we performed liquid culture of BM cells in the presence of TPO and counted cells stained with AchE after 3 days of culture. The number of megakaryocyte progenitors in mutant BM was also reduced

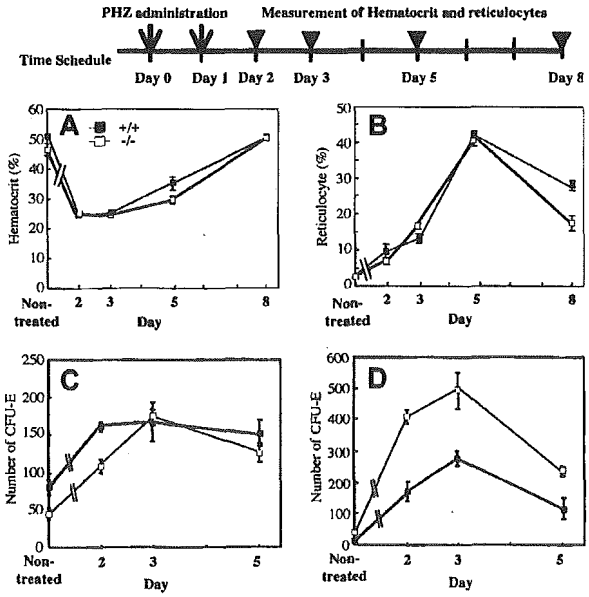

Figure 4. Kinetics of recovery after acute hemolysis by phenylhydrazine administration. A single dose of phenylhydrazine (60 mg/kg body weight) was administered intraperitoneally on days 0 and 1 (arrows). Wild-type and mutant mice were killed at 1, 2, 4, or 7 days after the final administration (arrowheads). Recovery was monitored by measurement of hematocrit (A) and reticulocytes (B). CFU-Es (mean ± SD) of 25 000 BM nucleated cells (C) and 100 000 spleen nucleated cells (D) from wild-type and mutant mice on days 2, 3, and 5 (n = 3 to 5 for each genotype) were assessed by semisolid methylcellulose cultures.

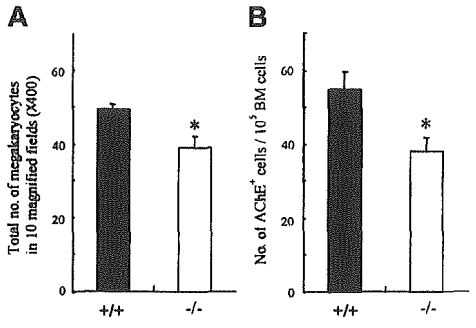

Figure 5. Megakaryocyte and its progenitor from BM of OSMR$^{+/+}$ and OSMR$^{-/-}$ mice. (A) The sections of femora from OMSR$^{-/-}$ and OSMR$^{-/-}$ mice were stained with hematoxylin and eosin. (A) The number of mature megakaryocytes in 10 fields (original magnification, × 40) of femoral sections was counted. Error bars indicate mean ± SD, n = 3 of each genotype. (B) Megakaryocytic progenitors were assessed by liquid culture of BM. BM nucleated cells (100 000 cells) were incubated in IMDM containing 1% Nutridoma SP and TPO at 25 ng/mL in 96-well plate at 37°C supplemented with 5% CO_2 for 3 days. The number of mature megakaryocytes identified by AchE staining was counted (mean ± SD, n = 7 of each genotype). *$P < .05$ between wild-type and mutant mice.

(Figure 5B). These data suggested that the reduced peripheral platelet number in mutant mice was in part due to the decrease of megakaryocyte progenitors, CFU-GEMMs and CFU-MEs, in BM, whereas it still remains possible that OSM affects the maturation process of megakaryocytes.

Transplantation of OSMR$^{+/+}$ hematopoietic stem cells in OSMR$^{-/-}$ mice

OSMR$^{-/-}$ mice showed impaired hematopoiesis in BM, whereas hematopoiesis in the spleen increased. However, the mechanism of the OSM effects on hematopoiesis remained unclear. To determine whether OSM affects immature hematopoietic progenitors directly or indirectly through acting on their microenvironments such as BM stromal cells, we transplanted wild-type hematopoietic stem cells (HSCs) into OSMR$^{-/-}$ mice. If OSM directly stimulates the hematopoietic progenitors, but not the microenvironment in BM, the engrafted wild-type HSCs in the BM of OSMR$^{-/-}$ mice should proliferate and recover to the normal level of progenitors. To address this question, lineage-negative BM cells from transgenic mice constitutively expressing GFP were injected into the livers of busulfan-treated neonatal mice[26,29] (Figure 6A). OSMR$^{-/-}$ GFP-positive BM cells as well as OSMR$^{+/+}$ GFP-positive BM cells were injected into OSMR$^{-/-}$ neonates. Donor contribution in the recipient mice was examined by flow cytometric analysis of the peripheral blood (Figure 6B). Wild-type GFP-transgenic mice were used as OSMR$^{+/+}$ controls. Eight and 7 recipients were engrafted with wild-type and mutant BM cells, respectively. Four and 5 of those mice that showed relatively high donor contribution were used for the following analysis (Table 1). Hematologic analysis of these mice revealed that engraftment of wild-type lineage-negative BM cells into OSMR$^{-/-}$ mice failed to increase the numbers of red

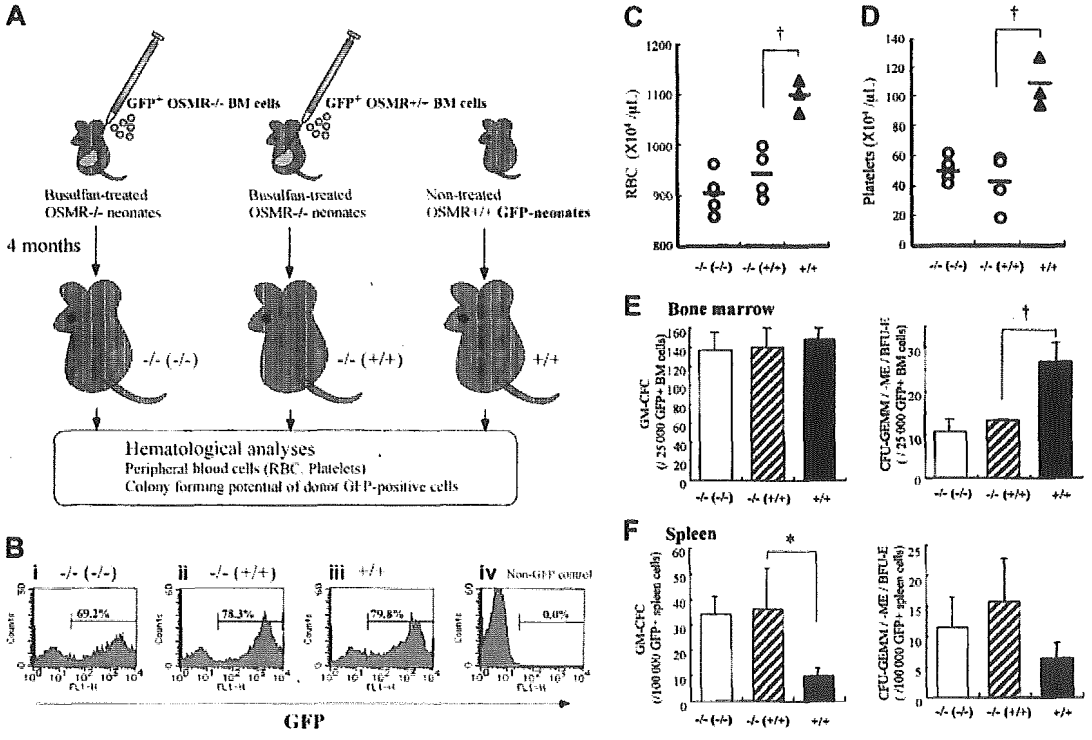

Figure 6. Transplantation of BM cells in OSMR$^{-/-}$ mice. (A) To investigate whether wild-type hematopoietic cells are able to convert the hematologic profile of mutant mice to the wild type, BM cells were transplanted into busulfan-treated neonatal OSMR$^{-/-}$ mice. To distinguish donor cells from recipients, BM cells from GFP-transgenic mouse were used as input cells. $^{/}$ ($^{/}$) indicates OSMR $^{/}$ mice reconstituted with BM cells of GFP-transgenic OSMR $^{/}$ mouse; $^{/}$ ($^{/+/+}$), OSMR $^{/}$ mice reconstituted with BM cells of GFP-transgenic OSMR$^{+/+}$ mouse; and $^{-/-}$, GFP-transgenic OSMR$^{-/+}$ mice. Recipient mice were killed 4 months after transplantation and the levels of donor contribution in peripheral blood were determined by FACS. Of fifteen recipient mice, 4 or 5 mice exhibiting relatively high proportion of donor type were used for the following hematologic analyses. (B) Representative FACS profiles of a mouse from each group. (i) $^{-/-}$ ($^{-/-}$); (ii) $^{-/-}$ ($^{+/+}$); (iii) $^{+/-}$; and (iv) non-GFP control. (C-D) Hematologic analyses of the reconstituted OSMR$^{-/-}$ mice and wild-type GFP mice. Orbital plexus blood was collected from anesthetized mice. Peripheral RBCs (C) and platelets (D) were analyzed by using automated counter Sysmex K-4500. The horizontal bar represents the mean. (E-F) GFP-positive donor cells were sorted from BM (E) and spleen (F) of each engrafted recipient mouse. GFP-transgenic wild-type mouse was used as OSMR$^{-/-}$ control. The hematopoietic progenitor content (GM-CFCs, left panel; and CFU-GEMMs/CFU-MEs/BFU-Es, right panel) of the sorted donor BM and spleen cells was assessed. The figure represents the mean ± SD [n = 4 for $^{/}$ ($^{/}$), n = 4 for $^{/}$ ($^{+/+}$) and n = 3 for $^{+/-}$]. *$P < .05$ between wild-type and mutant mice. †$P < .01$ between wild-type and mutant mice.

Table 1. Donor contribution in recipient mouse engrafted with wild-type cells

Mouse type	GFP-positive donor cells (%)
GFP mouse	79.8 (100)
Mutant mice engrafted with wild-type BM	
Mouse 1	78.3 (98.1)
Mouse 2	46.9 (58.8)
Mouse 3	19.9 (24.9)
Mouse 4	19.8 (24.8)
Mutant mice engrafted with mutant BM	
Mouse 1	69.2 (86.7)
Mouse 2	56.2 (70.4)
Mouse 3	45.8 (57.4)
Mouse 4	44.7 (56.0)
Mouse 5	44.0 (55.1)

The proportion of GFP-positive donor cells (%) was measured by FACS.
In 100% chimerism of GFP mouse, the converted number was put in parentheses.

blood cells and platelets in peripheral blood (Figure 6C-D), suggesting that the hematopoietic microenvironments must be altered in OSMR$^{-/-}$ mice. To verify the hematopoietic potential of the engrafted cells, the donor-derived GFP-positive cells were sorted by FACS and were subjected to semisolid colony assays. The colony-forming potential of GFP-positive OSMR$^{+/+}$ cells in mutant recipients was not increased, indicating that the hematopoietic potential depends on the environment of the recipient (Figure 6E-F). These results indicated that OSM affected BM hematopoiesis indirectly, possibly acting on the BM stromal cells that constitute the hematopoietic microenvironment. However, the results do not preclude the possibility that OSM affects the hematopoietic cells directly, which has been shown in vitro experiments.[45]

Transplantation of OSMR$^{-/-}$ hematopoietic stem cells in OSMR$^{+/+}$ mice

In order to test whether OSM directly acts on hematopoietic progenitors, we performed the reciprocal experiment (ie, transplantation of mutant HSCs in OSMR$^{+/+}$ mice). If OSM also stimulates the hematopoietic progenitors directly, the engrafted OSMR$^{-/-}$ HSCs in the wild-type BM would exhibit impaired hematologic properties similar to the OSMR-deficient mice. To assess the property of OSMR$^{-/-}$ hematopoietic cells in OSMR$^{+/+}$ mice, the effect of the endogenous OSMR$^{+/+}$ hematopoietic cells should be excluded. For this reason, evaluation of transplanted cells requires nearly complete chimerism of the transplanted HSCs. Two mice with high donor contribution were used for the following analysis

Table 2. Donor contribution in recipient mouse engrafted with mutant BM cells

Mouse type	GFP-positive donor cells (%)
GFP mouse	85.7 (100)
Wild-type mouse engrafted with mutant BM	
Mouse 1	81.2 (94.7)
Mouse 2	80.8 (94.2)
Wild-type mouse engrafted with wild-type BM	
Mouse 1	54.8 (63.9)
Mouse 2	48.3 (56.4)
Mouse 3	34.5 (40.2)
Mouse 4	23.4 (27.3)

The proportion of GFP-positive donor cells (%) was measured by FACS.
In 100% chimerism of GFP mouse, the converted number was put in parentheses.

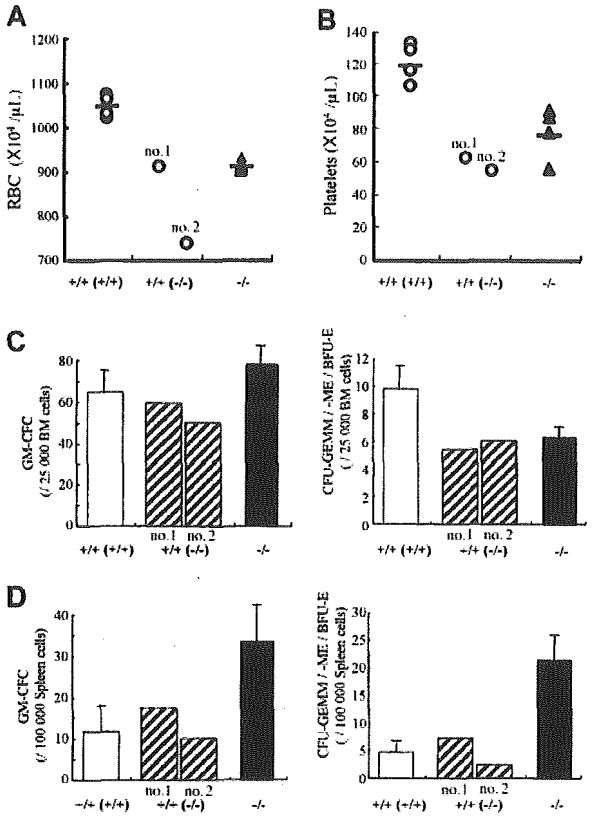

Figure 7. Transplantation of BM cells in OSMR$^{+/+}$ mice. OSMR$^{+/+}$ or OSMR$^{-/-}$ GFP-positive BM cells were transplanted into busulfan-treated neonatal OSMR$^{-/-}$ mice. $^{+/+}$ ($^{-/-}$) indicates OSMR$^{+/-}$ mice reconstituted with BM cells of GFP-transgenic OSMR$^{+/+}$ mouse; $^{+/-}$ ($^{-/-}$), OSMR$^{-/+}$ mice reconstituted with BM cells of GFP-transgenic OSMR$^{-/-}$ mouse; and $^{-/-}$, GFP-transgenic OSMR$^{-/-}$ mice. Recipient mice were killed 4 months after transplantation and the levels of donor contribution in peripheral blood were determined by FACS. Four $^{-/+}$ ($^{+/-}$) mice exhibiting relatively high proportion of donor-type and 2 $^{+/+}$ ($^{-/-}$) mice (nos. 1 and 2) exhibiting high chimerism were used for the following hematologic analyses. Orbital plexus blood was collected from anesthetized mice. Peripheral RBCs (A) and platelets (B) were analyzed by using automated counter Sysmex K-4500. The horizontal bar represents the mean. (C-D) The hematopoietic progenitor content (GM-CFCs, left panel; and CFU-GEMMs/CFU-MEs/BFU-Es, right panel) of the BM (C) and spleen (D) cells were assessed. The figure represents the mean ± SD [n = 4 for $^{+/-}$ ($^{-/+}$) and $^{-/-}$] and each value for $^{+/+}$ ($^{-/-}$).

(Table 2). Hematologic analysis revealed that both mice reconstituted with mutant HSCs exhibited a phenotype similar to mutant mice (Figure 7A-B), suggesting that OSM might also affect hematopoietic cells directly in normal hematopoiesis. To verify the hematopoietic potential of the engrafted cells, semisolid colony assay was performed. In this case, BM and spleen cells without sorting were used for the colony assay because of high chimerism. In agreement with the high chimerism of mutant hematopoietic cells, almost all colonies were fluorescent under the fluorescent microscopy, indicating that the engrafted mutant hematopoietic cells contributed to nearly all hematopoietic cells in the recipient mouse. The colony-forming potential of the engrafted mutant cells in BM exhibited the mutant phenotype (ie, reduced numbers of erythrocytic and megakaryocytic progenitors in BM, whereas the GM-CFC number was unchanged [Figure 7C]). These data suggested that OSM might affect the hematopoietic cells directly. Interestingly, hematopoietic progenitors in spleen of the wild-type mice that received OSMR-deficient BM cells exhibited phenotype similar to wild-type mice (Figure 7D).

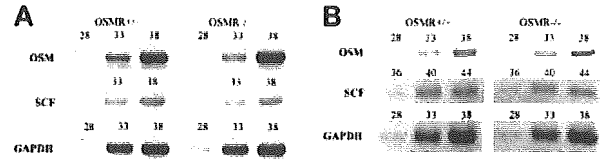

Figure 8. Semiquantitative RT-PCR analysis of OSM and SCF genes. One microgram of total RNA derived from BM (A) and spleen (B) of 3 mice was used to generate cDNA. Gene-specific primers for OSM, SCF, and GAPDH as control were used for PCR. The number represents PCR cycles of each sample.

However, if OSM is regulated through the OSMR signaling itself, the interpretation of transplant experiments would be more complex. To test this possibility, we examined the expression of OSM in OSMR$^{-/-}$ BM and spleen by semiquantitative RT-PCR and found that OSM expression was unaltered in OSMR-deficient mice, precluding the possibility (Figure 8). Similarly, as stem cell factor (SCF) is an important cytokine for hematopoiesis including megakaryopoiesis,[46] we compared the expression of SCF in OSMR$^{+/+}$ and OSMR$^{-/-}$ BM and spleen and found no significant difference, suggesting that SCF expression is independent of OSMR signaling.

Discussion

Signal transduction of IL-6–family cytokines is elicited by homodimerization of gp130 by IL-6 and IL-11 and heterodimerization of gp130 and LIFR by LIF, CNTF, and cardiotrophin-1. While heterodimerization of gp130 and OSMR is induced by OSM,[47] it remained possible that other cytokines also use the OSMR. Relatively mild defects were found in mice with a mutation of individual cytokines of this family due to functional overlap among the family members. In contrast, the disruption of the shared components of the receptors, gp130 or LIFR, leads to severe phenotype and mortality because this inactivates functions of multiple cytokines simultaneously.[48,49] Since the box1 and box2 regions, which contribute to downstream signaling cascade, are present in the intracellular domain of OSMR,[30] OSMR itself is also a signal transducing molecule. Therefore, it was possible that the disruption of OSMR might cause severe defects if OSMR is used by another novel cytokine. However, the hematologic characteristics in OSMR$^{-/-}$ mice were similar to those in OSM$^{-/-}$ mice (K. Minehata, manuscript in preparation), suggesting that OSMR is not shared by other cytokines.

The overlapping functions of the IL-6–family cytokines are explained by the shared signal transducer gp130.[1] Especially OSM and LIF display many similar biologic activities.[5,9,50] OSM and LIF are not only structurally related but their genes are also tightly linked in the same chromosomal location, suggesting that the 2 genes arose by duplication.[4] Moreover, the OSMR gene was also found to be located in the vicinity of the LIFR locus in mouse.[30] Actually, OSM and LIF share the same LIF receptor in human.[12] Therefore, OSM had long been considered as just another LIF. It has been reported that LIF-deficient mice display female sterility due to defective blastocyst implantation, postnatal growth retardation, and defects in hematopoiesis and thymocyte proliferation.[40] While the levels of circulating mature red blood cells and platelets, as well as the numbers of BFU-Es and GM-CFCs in the BM, were normal in LIF$^{-/-}$ mice, the numbers of BFU-Es and GM-CFCs in the spleen of LIF$^{-/-}$ mice were significantly decreased compared with wild-type mice. These results are quite different from what we found in OSMR$^{-/-}$ mice as shown in Figure 3 (ie, BFU-Es and CFU-Es in BM were reduced, whereas they were increased in spleen). Hematologic characteristics in IL-6$^{-/-}$ mice were also different from OSMR$^{-/-}$ mice[38] (ie, the number of BFU-Es was increased in the BM of IL-6$^{-/-}$ mice compared with wild-type mice), whereas enhanced hematopoiesis in the IL-6$^{-/-}$ spleen was similar to OSMR$^{-/-}$ mice. Thus, mice lacking either LIF, IL-6, or OSMR display a distinct pattern of hematopoiesis, although all the IL-6–family cytokines use gp130 as the common signal transducer. The complex response is likely to reflect a complex interaction between the cytokines and their receptors in this family and compensatory mechanisms that affect hematopoietic systems directly or indirectly.

It is known that the IL-6–family cytokines are involved in megakaryopoiesis in vitro and in vivo. Although IL-6, IL-11, LIF, and OSM enhanced the megakaryocytic colony formation in synergy with other cytokines such as IL-3 or TPO, they had little or no such activity alone[32-34,45] and they rather appear to stimulate the maturation of megakaryocytes in vitro by increasing size and ploidy. In vivo, the administration of these cytokines elevated numbers of megakaryocytes and platelets.[35-37,45] However, mice lacking either IL-6, LIF, or the specific IL-11 receptor α-chain are not thrombocytopenic despite these activities,[38-40] indicating functional redundancy among these cytokines in megakaryopoiesis. Unlike these mice, the number of peripheral platelets was reduced in OSMR$^{-/-}$ mice, suggesting that OSM plays an important role for megakaryopoiesis under the steady-state condition. Since transplantation of OSMR-deficient BM cells into wild-type mice resulted in the reduction of peripheral platelets, OSM might directly affect the maturation of megakaryocytes in vivo as described in the previous in vitro study.[45] Consistently, immunohistochemical analysis revealed that CD41^{+} megakaryocytic cells expressed OSMR (K. Minehata, manuscript in preparation).

Recently, Broxmeyer et al[51] reported that the number of hematopoietic progenitors in Stat4$^{-/-}$ mice was significantly reduced and recovered by T-cell–specific transgenic expression of Stat4. Furthermore, the injection of a Th1 cytokine OSM, but not other cytokines, into Stat4$^{-/-}$ mice recovered progenitor cell activity to wild-type levels. Based on these results they suggested that OSM is a potential mediator between T cells and hematopoietic progenitors. These data are also consistent with our findings that OSMR$^{-/-}$ mice exhibit impaired homeostasis.

Considering the results of BM transplantation, OSM is likely to be involved in hematopoietic homeostasis by acting on the BM stromal cells. OSM is a proinflammatory as well as an anti-inflammatory cytokine depending on the cellular context. An important characteristic of OSM is its potent activity to induce tissue inhibitor of metalloproteinases (TIMPs). Matrix metalloproteinases (MMPs) are involved in extracellular matrix breakdown during inflammatory reactions and TIMPs inhibit their function. Therefore, the balance between MMPs and TIMPs is important for the remodeling of the extracellular matrix. Among the IL-6–family cytokines, OSM selectively stimulates the expression of TIMP-1 in fibroblasts[19,52] and synovial lining cells.[53] The marked induction of TIMP-1 by OSM indicates that the OSM-specific receptor is required for the full spectrum of TIMP-1 expression. In fact, the recovery from liver injury was delayed in OSMR$^{-/-}$ mice that showed impaired TIMP-1 expression and prolonged activation of MMP-9 (K. Nakamura, submitted). Thus, the regulation of MMP-9 and TIMP-1 by OSM may play an important role for the maintenance of BM microenvironment. Recently, Heissig et al[54]

reported that MMP-9$^{-/-}$ mice failed to recover hematopoiesis after BM ablation because of the defective release of soluble SCF and HSC mobilization from BM. Therefore, we presumed alteration of the SCF level in mutant mice. However, OSMR signaling was not required for expression of SCF at transcriptional and serum protein levels (Figure 8; K. Minehata, manuscript in preparation). It is therefore likely that OSM regulates expression of the other cytokines or membrane-bound proteins that constitute the BM microenvironment.

In contrast to BM, hematopoietic progenitors in spleen of OSMR$^{-/-}$ were increased compared with OSMR$^{+/+}$ mice. Hematopoietic progenitors in spleen were increased in OSMR-deficient mice that received either wild-type or OSMR-deficient BM cells, whereas they were not increased in the wild-type mice that received either wild-type or OSMR-deficient BM cells. These results suggest that OSM affects the splenic hematopoietic microenvironment rather negatively.

In conclusion, our results indicate that OSMR$^{-/-}$ mice exhibit unique hematologic characteristics that have not been recognized in mice defective in functions of either IL-6, IL-11, LIF, or CNTF and that OSM regulates hematopoiesis in BM and spleen by acting on both stromal cells and erythrocytic and megakaryocytic progenitors.

Acknowledgments

We are grateful to Drs S. Takahashi and M. Okabe for providing us with vectors and GPF transgenic mice, respectively.

References

1. Kishimoto T, Akira S, Taga T. Interleukin-6 and its receptor: a paradigm for cytokines. Science. 1992;258:593-597.
2. Hibi M, Nakajima K, Hirano T. IL-6 cytokine family and signal transduction: a model of the cytokine system. J Mol Med. 1996;74:1-12.
3. Senaldi G, Varnum BC, Sarmiento U, et al. Novel neurotrophin-1/B cell-stimulating factor-3: a cytokine of the IL- 6 family. Proc Natl Acad Sci U S A. 1999;96:11458-11463.
4. Jeffery E, Price V, Gearing DP. Close proximity of the genes for leukemia inhibitory factor and oncostatin M. Cytokine. 1993;5:107-111.
5. Rose TM, Weiford DM, Gunderson NL, Bruce AG. Oncostatin M (OSM) inhibits the differentiation of pluripotent embryonic stem cells in vitro. Cytokine. 1994;6:48-54.
6. Zarling JM, Shoyab M, Marquardt H, Hanson MB, Lioubin MN, Todaro GJ. Oncostatin M: a growth regulator produced by differentiated histiocytic lymphoma cells. Proc Natl Acad Sci U S A. 1986; 83:9739-9743.
7. Brown TJ, Lioubin MN, Marquardt H. Purification and characterization of cytostatic lymphokines produced by activated human T lymphocytes: synergistic antiproliferative activity of transforming growth factor beta 1, interferon-gamma, and oncostatin M for human melanoma cells. J Immunol. 1987;139:2977-2983.
8. Malik N, Kallestad JC, Gunderson NL, et al. Molecular cloning, sequence analysis, and functional expression of a novel growth regulator, oncostatin M. Mol Cell Biol. 1989;9:2847-2853.
9. Bruce AG, Hoggatt IH, Rose TM. Oncostatin M is a differentiation factor for myeloid leukemia cells. J Immunol. 1992;149:1271-1275.
10. Murakami-Mori K, Taga T, Kishimoto T, Nakamura S. AIDS-associated Kaposi's sarcoma (KS) cells express oncostatin M (OM)- specific receptor but not leukemia inhibitory factor/OM receptor or interleukin-6 receptor: complete block of OM-induced KS cell growth and OM binding by anti-gp130 antibodies. J Clin Invest. 1995;96:1319-1327.
11. Cichy J, Rose-John S, Travis J. Oncostatin M, leukaemia-inhibitory factor and interleukin 6 trigger different effects on alpha1-proteinase inhibitor synthesis in human lung-derived epithelial cells. Biochem J. 1998;329:335-339.
12. Gearing DP, Bruce AG. Oncostatin M binds the high-affinity leukemia inhibitory factor receptor. New Biol. 1992;4:61-65.
13. Gearing DP, Comeau MR, Friend DJ, et al. The IL-6 signal transducer, gp130: an oncostatin M receptor and affinity converter for the LIF receptor. Science. 1992;255:1434-1437.
14. Thoma B, Bird TA, Friend DJ, Gearing DP, Dower SK. Oncostatin M and leukemia inhibitory factor trigger overlapping and different signals through partially shared receptor complexes. J Biol Chem. 1994;269:6215-6222.
15. Mosley B, De Imus C, Friend D, et al. Dual oncostatin M (OSM) receptors: cloning and characterization of an alternative signaling subunit conferring OSM-specific receptor activation. J Biol Chem. 1996;271:32635-32643.
16. Modur V, Feldhaus MJ, Weyrich AS, et al. Oncostatin M is a proinflammatory mediator: in vivo effects correlate with endothelial cell expression of inflammatory cytokines and adhesion molecules. J Clin Invest. 1997;100:158-168.
17. Cichy J, Potempa J, Chawla RK, Travis J. Regulation of alpha 1-antichymotrypsin synthesis in cells of epithelial origin. FEBS Lett. 1995;359: 262-266.
18. Bellido T, Stahl N, Farruggella TJ, Borba V, Yancopoulos GD, Manolagas SC. Detection of receptors for interleukin-6, interleukin-11, leukemia inhibitory factor, oncostatin M, and ciliary neurotrophic factor in bone marrow stromal/osteoblastic cells. J Clin Invest. 1996;97:431-437.
19. Richards CD, Kerr C, Tanaka M, et al. Regulation of tissue inhibitor of metalloproteinase-1 in fibroblasts and acute phase proteins in hepatocytes in vitro by mouse oncostatin M, cardiotrophin-1, and IL-6. J Immunol. 1997;159:2431-2437.
20. Tamura S, Morikawa Y, Tanaka M, Miyajima A, Senba E. Developmental expression pattern of oncostatin M receptor beta in mice. Mech Dev. 2002;115:127-131.
21. Ichihara M, Hara T, Kim H, Murate T, Miyajima A. Oncostatin M and leukemia inhibitory factor do not use the same functional receptor in mice. Blood. 1997;90:165-173.
22. Yoshimura A, Ichihara M, Kinjyo I, et al. Mouse oncostatin M: an immediate early gene induced by multiple cytokines through the JAK-STAT5 pathway. EMBO J. 1996;15:1055-1063.
23. Mukouyama Y, Hara T, Xu M, et al. In vitro expansion of murine multipotential hematopoietic progenitors from the embryonic aorta-gonad-mesonephros region. Immunity. 1998;8:105-114.
24. Kamiya A, Kinoshita T, Ito Y, et al. Fetal liver development requires a paracrine action of oncostatin M through the gp130 signal transducer. EMBO J. 1999;18:2127-2136.
25. Miyajima A, Kinoshita T, Tanaka M, Kamiya A, Mukouyama Y, Hara T. Role of Oncostatin M in hematopoiesis and liver development. Cytokine Growth Factor Rev. 2000;11:177-183.
26. Okabe M, Ikawa M, Kominami K, Nakanishi T, Nishimune Y. 'Green mice' as a source of ubiquitous green cells. FEBS Lett. 1997;407:313-319.
27. Minehata K, Mukouyama YS, Sekiguchi T, Hara T, Miyajima A. Macrophage colony stimulating factor modulates the development of hematopoiesis by stimulating the differentiation of endothelial cells in the AGM region. Blood. 2002;99:2360-2368.
28. Jackson CW. Cholinesterase as a possible marker for early cells of the megakaryocytic series. Blood. 1973;42:413-421.
29. Yoder MC, Hiatt K, Dutt P, Mukherjee P, Bodine DM, Orlic D. Characterization of definitive lymphohematopoietic stem cells in the day 9 murine yolk sac. Immunity. 1997;7:335-344.
30. Tanaka M, Hara T, Copeland NG, Gilbert DJ, Jenkins NA, Miyajima A. Reconstitution of the functional mouse oncostatin M (OSM) receptor: molecular cloning of the mouse OSM receptor beta subunit. Blood. 1999;93:804-815.
31. Hara T, Tamura K, de Miguel MP, et al. Distinct roles of oncostatin M and leukemia inhibitory factor in the development of primordial germ cells and sertoli cells in mice. Dev Biol. 1998;201:144-153.
32. Ishibashi T, Kimura H, Uchida T, Kariyone S, Friese P, Burstein SA. Human interleukin 6 is a direct promoter of maturation of megakaryocytes in vitro. Proc Natl Acad Sci U S A. 1989;86:5953-5957.
33. Burstein SA, Mei RL, Henthorn J, Friese P, Turner K. Leukemia inhibitory factor and interleukin-11 promote maturation of murine and human megakaryocytes in vitro. J Cell Physiol. 1992; 153:305-312.
34. Metcalf D, Hilton D, Nicola NA. Leukemia inhibitory factor can potentiate murine megakaryocyte production in vitro. Blood. 1991;77:2150-2153.
35. Ishibashi T, Kimura H, Shikama Y, et al. Interleukin-6 is a potent thrombopoietic factor in vivo in mice. Blood. 1989;74:1241-1244.
36. Neben TY, Loebelenz J, Hayes L, et al. Recombinant human interleukin-11 stimulates megakaryocytopoiesis and increases peripheral platelets in normal and splenectomized mice. Blood. 1993; 81:901-908.
37. Metcalf D, Nicola NA, Gearing DP. Effects of injected leukemia inhibitory factor on hematopoietic and other tissues in mice. Blood. 1990;76:50-56.
38. Bernad A, Kopf M, Kulbacki R, Weich N, Koehler G, Gutierrez-Ramos JC. Interleukin-6 is required in vivo for the regulation of stem cells and committed progenitors of the hematopoietic system. Immunity. 1994;1:725-731.
39. Nandurkar HH, Robb L, Tarlinton D, Barnett L, Kontgen F, Begley CG. Adult mice with targeted mutation of the interleukin-11 receptor (IL11Ra) display normal hematopoiesis. Blood. 1997;90: 2148-2159.
40. Escary JL, Perreau J, Dumenil D, Ezine S, Brulet P. Leukaemia inhibitory factor is necessary for maintenance of haematopoietic stem cells and thymocyte stimulation. Nature. 1993;363:361-364.

41. Vannucchi AM, Paoletti F, Linari S, et al. Identification and characterization of a bipotent (erythroid and megakaryocytic) cell precursor from the spleen of phenylhydrazine-treated mice. Blood. 2000;95:2559-2568.

42. Lerner C, Harrison DE. 5-fluorouracil spares hemopoietic stem cells responsible for long-term repopulation. Exp Hematol. 1990;18:114-118.

43. Zucker-Franklin D, Petursson S. Thrombocytopoiesis—analysis by membrane tracer and freeze-fracture studies on fresh human and cultured mouse megakaryocytes. J Cell Biol. 1984; 99:390-402.

44. Choi ES, Nichol JL, Hokom MM, Hornkohl AC, Hunt P. Platelets generated in vitro from proplatelet-displaying human megakaryocytes are functional. Blood. 1995;85:402-413.

45. Wallace PM, MacMaster JF, Rillema JR, Peng J, Burstein SA, Shoyab M. Thrombocytopoietic properties of oncostatin M. Blood. 1995;86:1310-1315.

46. Tanaka R, Koike K, Imai T, et al. Stem cell factor enhances proliferation, but not maturation, of murine megakaryocytic progenitors in serum-free culture. Blood. 1992;80:1743-1749.

47. Heinrich PC, Behrmann I, Muller-Newen G, Schaper F, Graeve L. Interleukin-6-type cytokine signalling through the gp130/Jak/STAT pathway. Biochem J. 1998;334:297-314.

48. Yoshida K, Taga T, Saito M, et al. Targeted disruption of gp130, a common signal transducer for the interleukin 6 family of cytokines, leads to myocardial and hematological disorders. Proc Natl Acad Sci U S A. 1996;93:407-411.

49. Ware CB, Horowitz MC, Renshaw BR, et al. Targeted disruption of the low-affinity leukemia inhibitory factor receptor gene causes placental, skeletal, neural and metabolic defects and results in perinatal death. Development. 1995;121:1283-1299.

50. Piquet-Pellorce C, Grey L, Mereau A, Heath JK. Are LIF and related cytokines functionally equivalent? Exp Cell Res. 1994;213:340-347.

51. Broxmeyer HE, Bruns HA, Zhang S, et al. Th1 cells regulate hematopoietic progenitor cell homeostasis by production of oncostatin M. Immunity. 2002;16:815-825.

52. Richards CD, Shoyab M, Brown TJ, Gauldie J. Selective regulation of metalloproteinase inhibitor (TIMP-1) by oncostatin M in fibroblasts in culture. J Immunol. 1993;150:5596-5603.

53. Gatsios P, Haubeck HD, Van de Leur E, et al. Oncostatin M differentially regulates tissue inhibitors of metalloproteinases TIMP-1 and TIMP-3 gene expression in human synovial lining cells. Eur J Biochem. 1996;241:56-63.

54. Heissig B, Hattori K, Dias S, et al. Recruitment of stem and progenitor cells from the bone marrow niche requires MMP-9 mediated release of kit-ligand. Cell. 2002;109:625-637.

Development 130, 4259-4268

doi:10.1242/dev.00629

Feedback loops comprising Dll1, Dll3 and Mesp2, and differential involvement of Psen1 are essential for rostrocaudal patterning of somites

Yu Takahashi[1], Tohru Inoue[1], Achim Gossler[2] and Yumiko Saga[3,*]

[1]Cellular and Molecular Toxicology Division, National Institute of Health Sciences, 1-18-1 Kamiyoga, Setagayaku, Tokyo 158-8501, Japan
[2]Institut für Molekularbiologie, MHH, 30625 Hannover, Germany
[3]Division of Mammalian Development, National Institute of Genetics, SOKENDAI, Yata 1111, Mishima 411-8540, Japan
*Author for correspondence (e-mail: ysaga@lab.nig.ac.jp)

Accepted 27 May 2003

SUMMARY

Elaborate metamerism in vertebrate somitogenesis is based on segmental gene expression in the anterior presomitic mesoderm (PSM). Notch signal pathways with Notch ligands Dll1 and Dll3, and the transcription factor Mesp2 are implicated in the rostrocaudal patterning of the somite. We have previously shown that changes in the *Mesp2* expression domain from a presumptive one somite into a rostral half somite results in differential activation of two types of Notch pathways, dependent or independent of presenilin 1 (Psen1), which is a Notch signal mediator. To further refine our hypothesis, we have analyzed genetic interactions between *Dll1*, *Dll3*, *Mesp2* and *Psen1*, and elucidated the roles of Dll1- and Dll3-Notch pathways, with or without Psen1, in rostrocaudal patterning. Dll1 and Dll3 are co-expressed in the PSM and so far are considered to have partially redundant functions. We find in this study that positive and negative feedback loops comprising Dll1 and Mesp2 appear to be crucial for this patterning, and Dll3 may be required for the coordination of the Dll1-Mesp2 loop. Additionally, our epistatic analysis revealed that Mesp2 affects rostrocaudal properties more directly than Dll1 or Dll3. Finally, we find that Psen1 is involved differently in the regulation of rostral and caudal genes. Psen1 is required for Dll1-Notch signaling for activation of *Dll1*, while the Psen1-independent Dll3-Notch pathway may counteract the Psen1-dependent Dll1-Notch pathway. These observations suggest that Dll1 and Dll3 may have non-redundant, even counteracting functions. We conclude from our analyses that Mesp2 functions as a central mediator of such Notch pathways and regulates the gene expression required for rostrocaudal patterning of somites.

Supplemental data available online

Key words: Mesp2, Notch signaling, Rostrocaudal patterning, Presenilin, Somite segmentation, Mouse

INTRODUCTION

Somitogenesis is an intriguing example of metameric pattern formation in vertebrate embryos. Epithelial somites form at the anterior end of the unsegmented paraxial mesoderm, which is supplied by the primitive streak or tail bud, by a mesenchymal-epithelial conversion in a spatially and temporally coordinated manner. Each somite is subdivided into two compartments, the rostral (anterior) and caudal (posterior) halves. This rostrocaudal polarity appears to be established just prior to somite formation.

Studies in zebrafish, chick and mouse embryos have established that the Notch signaling pathway is essential for somite formation and patterning, particularly for the establishment of the rostrocaudal segment polarity (Conlon et al., 1995; Oka et al., 1995; Dornseifer et al., 1997; Hrabe de Angelis et al., 1997; Wong et al., 1997; Kusumi et al., 1998; Evrard et al., 1998; Zhang and Gridley, 1998; del Barco Barrantes et al., 1999; Takke and Campos-Ortega, 1999; Holley et al., 2000; Takahashi et al., 2000; Koizumi et al., 2001; Bessho et al., 2001) (reviewed by Saga and Takeda, 2001). In fact, many zebrafish and mouse mutants for genes encoding Notch pathway components exhibit defects in the rostrocaudal polarity of somites. The Notch signaling is closely linked to the putative molecular clock mechanism that operates in the PSM, as oscillating genes encode Notch pathway components and mutations in Notch pathway components also affect cyclic genes (Palmeirim et al., 1997; McGrew et al., 1998; Forsberg et al., 1998; Jiang et al., 2000; Holley et al., 2002; Oates and Ho, 2002). The generation of the rostrocaudal polarity is also thought to be controlled by the molecular clock. However, the precise nature of the molecular clock is not yet known at all. In zebrafish, defects in the rostrocaudal polarity are often not distinguished from defects in the molecular clock function, because most of Notch pathway mutants in zebrafish exhibit similar phenotypes. For example, zebrafish *aei*, *des* and *bea* mutant embryos commonly show a salt-and-pepper (randomized) expression pattern of the rostral- or caudal-half marker genes, instead of normal regular stripes (Jiang et al., 2000; Holley et al., 2002). This phenotype is virtually

indistinguishable from the phenotype seen in the *her1*- and *her7*- Morpholino-injected embryo, which shows disruption of cyclic gene expression (Oates and Ho, 2002). Thus, there is no available Notch pathway mutant in zebrafish that enables further analysis of the mechanism of rostrocaudal patterning separately from the molecular clock.

By contrast, Notch pathway mutants in mouse exhibit various patterns of phenotypes regarding the rostrocaudal polarity of somites. For example, in Delta-like 1 (Dll1)- and RBPjk-null embryos, somites show neither rostral nor caudal property (del Barco Barrantes et al., 1999), whereas Delta-like 3 (Dll3), lunatic fringe and Hes7-null embryos show a salt-and-pepper expression pattern of caudal marker genes (Kusumi et al., 1998; Evrard et al., 1998; Zhang and Gridley, 1998; Bessho et al., 2001). In our previous work, we have demonstrated that Mesp2-null and presenilin 1 (Psen1)-null embryos show opposite phenotypes with respect to the rostrocaudal polarity of somites (Takahashi et al., 2000). The Mesp2-null embryo exhibits caudalized somites, i.e., the somite loses the rostral-half property, and the whole somite acquires the caudal-half characteristics. The reverse is true for the Psen1-null embryo. These observations led us to some fundamental questions: what is the default state, and how do these genes cooperate to establish rostrocaudal segment polarity? In some mouse mutants, such as Dll3-null, oscillation of cyclic genes is disrupted (Dunwoodie et al., 2002). However, in Mesp2-null embryos, the rostrocaudal polarity is disrupted without affecting oscillation of cyclic genes in the posterior PSM (Nomura-Kitabayashi et al., 2002) (Y.T., unpublished). In Psen1-null embryos, oscillation of cyclic genes in the posterior PSM normally occurs, although the level of expression is reduced (Koizumi et al., 2001). Therefore Mesp2 and Psen1 serve as good tools for exploring mechanisms of the rostrocaudal patterning independent of molecular clock function.

Mesp2 is a member of the Mesp family, a group of bHLH transcription factors, which is expressed in the anterior PSM just prior to somite formation and is essential for somite boundary formation as well as formation of the rostrocaudal polarity (Saga et al., 1997; Nomura-Kitabayashi et al., 2001). We have previously observed that the rostrocaudal polarity of somites correlates well with the spatial pattern and the level of expression of the Notch ligand *Dll1*. Genetic analyses of Mesp2-null, and Psen1-null mice, and mice carrying an activated *Notch1* in the *Mesp2* locus have led us to propose a model for rostrocaudal patterning, in which two Notch pathways can be active in the anterior PSM. One is the Psen1-dependent Notch pathway for inducing expression of *Dll1*, and the other is the Psen1-independent Notch pathway for suppressing expression of *Dll1*. Mesp2 normally suppresses the *Dll1*-inducing pathway and potentiates the *Dll1*-suppressing pathway in a region corresponding to one presumptive somite. When *Mesp2* expression becomes restricted to the presumptive rostral half, expression of *Dll1* is induced in the presumptive caudal half by the Psen1-dependent Notch pathway (Takahashi et al., 2000). However, the ligands for these two Notch pathways have not yet been identified.

In both zebrafish and mouse embryos, at least two Notch ligands (DeltaC and DeltaD, and Dll1 and Dll3, respectively) are co-expressed in the PSM, and their expression domains are finally segregated into the rostral or caudal half of formed somites (Bettenhausen et al., 1995; Dunwoodie et al., 1997; Haddon et al., 1998). These expression patterns imply that these ligands do not have merely redundant functions, but also have distinct roles in somite patterning and boundary formation. Despite a large number of studies, possible functional differences between Dll1 and Dll3 signals are not clear. Likewise, the roles of Psen1, a Notch signal mediator involved in nuclear translocation of the Notch intracellular domain (De Strooper et al., 1999; Struhl and Greenwald, 1999; Ye et al., 1999), during somitogenesis are not fully understood. If Psen1 were equally involved in all aspects of Notch signaling, it is puzzling that the rostrocaudal patterning defects of somites in the Psen1-null embryo are unique and different from that in any other Notch pathway mutants (Takahashi et al., 2000; Koizumi et al., 2001). Thus, to elucidate the precise requirements for Psen1 functions in somite patterning, further studies are required.

We have conducted genetic studies of the roles in rostrocaudal patterning of Dll1- and Dll3-mediated Notch signaling, the relationships between Notch signaling and Mesp2 function, and the involvement of Psen1 in Dll1- and Dll3-mediated Notch pathways. Our analysis of these genetic interactions revealed several novel findings.

(1) Dll1- and Dll3-Notch signaling and Mesp2 constitute a complex signaling network for stripe formation in the anterior PSM. Feedback loops of Dll1 and Mesp2 are essential for establishment of the rostrocaudal polarity, while Dll3 is necessary for localization and integration of expression of *Dll1* and *Mesp2*.

(2) Mesp2 can affect rostrocaudal properties more directly than Dll1 or Dll3.

(3) Psen1 is involved differently in Dll1-Notch and Dll3-Notch pathways.

(4) Dll3-Notch signaling can counteract Psen1-dependent Dll1-Notch signaling.

Based on these findings, we propose a new model for stripe formation in the anterior PSM, which is different from the previous hypothesis that rostrocaudal patterning, i.e. formation of the half-a-somite stripe pattern of gene expression, can be regarded as a result of stabilization of oscillating expression in the posterior PSM.

MATERIALS AND METHODS

Animals

The *Dll1*^{lacZ} knock-in (Hrabe de Angelis et al., 1997), *Mesp2*^{lacZ} knock-in (Takahashi et al., 2000), *Psen1*$^{-}$ (Koizumi et al., 2001) and *Dll3*^{pu} (Kusumi et al., 1998) mice are maintained in the animal facility in National Institute of Health Sciences, Japan. Double heterozygous mice with an ICR background for each combination of genes are used to obtain the double homozygous embryos. The primer sets used for genotyping are as shown in the original papers.

Analysis of phenotypes

The methods for gene expression analysis by whole-mount in situ hybridization, histology and skeletal preparation by Alcian Blue-Alizarin Red staining are as described in previous paper (Saga et al., 1997). A strong emphasis was placed on obtaining a precise and accurate comparison of gene expression patterns and intensity

of signals between different genotypes. Littermate embryos from crosses of double-heterozygous parents were simultaneously fixed and processed for in situ hybridization. Coloring reactions in BM purple solution (Roche) were stopped at exactly the same time for each embryo. To evaluate gene expression precisely in the double mutant embryo, simultaneous staining of wild-type and single mutant littermates as controls is essential. Therefore, in all of the images presented in the figures, the arranged embryos are littermates. At least four, but more usually six, double-null embryos were used for gene expression analysis with more than ten single mutants and many more wild-type embryos. Observed differences in gene expression levels were typically reproduced in triplicate. In the case of skeletal morphologies, each of eight Dll3/Mesp2 double-null fetuses exhibited almost complete fusion of neural arches. For vertebral morphologies in Dll3/Psen1 intercrosses, the number of fetuses is presented in supplementary data S2F. Each of six Dll3/Psen1 double-null fetuses showed reduced amounts of disorganized skeletal elements. Whole-mount specimens and skeletal preparations were observed and photographed with a Leica dissection microscope equipped with a Fujifilm digital camera (HC-2500) under specific illumination conditions.

RESULTS

Positive and negative feedback loops of Dll1 and Mesp2 are essential for stripe formation

We have demonstrated that suppression of *Dll1* by Mesp2 is essential for the establishment of rostrocaudal polarity and both activation and suppression of *Dll1* are mediated by Notch signaling through ligands which have not yet been defined. To address this question, we used mouse genetics to analyze the functional relationship between Dll1 and Mesp2. First we examined auto- and reciprocal regulations of *Dll1* and *Mesp2*. As the Dll1-null embryo has a *lacZ* knock-in allele (Hrabe de Angelis et al., 1997), we can observe expression of *Dll1-lacZ* in the absence of the Dll1 function. In the $Dll1^{+/L}$ embryo, *lacZ* expression reflects the normal expression pattern of *Dll1*, showing strong staining in the PSM and stripes in the caudal halves of somites (Fig. 1A,B). Sporadic expression in the neural tube is also noted. By contrast, in the $Dll1^{L/L}$ embryos, the *Dll1-lacZ* stripes are not

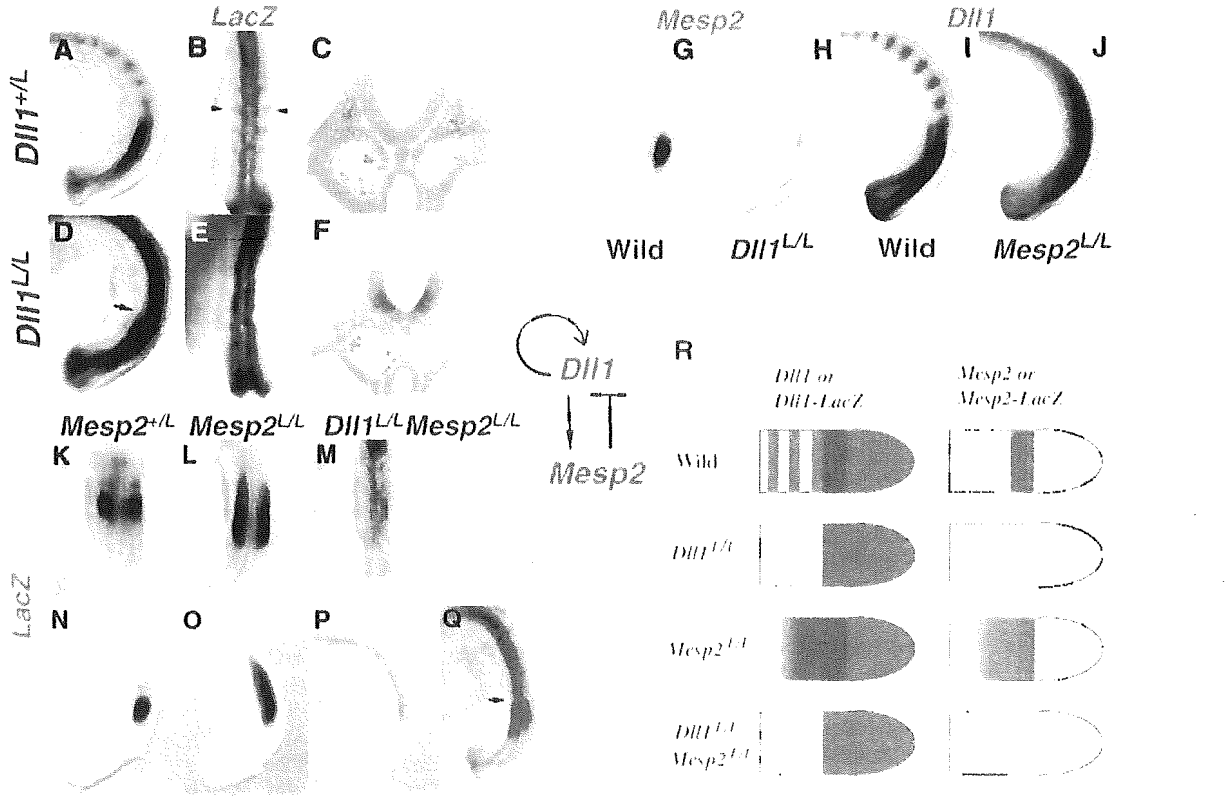

Fig. 1. Positive and negative feedback loops of Dll1 and Mesp2 are essential for stripe formation. (A-F) Dll1 induces expression of *Dll1* itself. Expression of *Dll1-lacZ* mRNA was detected by in situ hybridization in $Dll1^{+/L}$ (A-C) and $Dll1^{L/L}$ (D-F) embryos at 9.5 dpc. (A,D) Lateral view, (B,E) dorsal view of the tail region. (C,F) Transverse section at the anteriormost PSM. In the $Dll1^{L/L}$ embryo, *lacZ* expression reflects normal stripe pattern of *Dll1*, localized at the caudal half of somites (arrowheads in B). In the $Dll1^{L/L}$ embryo, the stripe of *Dll1-lacZ* is lost at the putative somite region (anterior to the arrow in D). Ectopic strong staining in the ventral neural tube is evident (F). (G-J) Expression of *Mesp2* is severely decreased in the Dll1-null embryo (G,H) while expression of *Dll1* is strongly expanded in the Mesp2-null embryo (I,J). (K-Q) *Mesp2-lacZ* mRNA (with *Dll1-lacZ* in case of the double mutant) was detected by in situ hybridization. (K-M) Dorsal views and (N-Q) lateral views. After extended staining, *Dll1-lacZ* expression appears at the neural tube and the PSM, but not at the somite region (Q, arrow indicates the putative boundary between PSM and somite region). (R) Summary of reciprocal regulation of *Dll1* and *Mesp2*. In the absence of Dll1, both *Dll1* stripes and normal level of *Mesp2* expression are lost. In the absence of Mesp2, both *Dll1* and *Mesp2-lacZ* expressions are strongly expanded. The Dll1/Mesp2 double-null embryo is similar to the Dll1-null embryo in terms of reciprocal regulation.

detected in the putative somite region, even after extended color development. Expression in the PSM appears not to be affected, but shows a sharp border in the anterior PSM (Fig. 1D,E, arrow in D'). It is noteworthy that strong and uniform *lacZ* expression is observed in the ventral neural tube, suggesting the lack of lateral inhibition (Fig. 1C,F). The different effects of the loss of Dll1 on *Dll1* transcription in the neural tube and somites suggest that the *Dll1* stripe formation in the rostral PSM is not a result of the lateral inhibition, but that Dll1 function itself is required for the formation of the *Dll1* stripes. Thus, Notch ligand that induces *Dll1* expression is Dll1 itself. However, *Dll1* expression in the posterior PSM seems to be independent of Dll1-Notch signaling. The loss of *Dll1-lacZ* stripes was also observed in the Dll1/Mesp2 double-null embryo, indicating that it is independent of the Mesp2 function (Fig. 1Q).

As reported previously (del Barco Barrantes et al., 1999), the expression of *Mesp2* is severely downregulated in the Dll1-null embryo (Fig. 1G,I), while strong expression of *Dll1* is expanded in the Mesp2-null embryo (Fig. 1I,J) (Takahashi et al., 2000). These observations indicate that Dll1 induces expression of *Dll1* itself and *Mesp2*, whereas Mesp2 suppresses expression of *Dll1*. This genetic cascade may propagate via the Dll1-Notch signaling pathway, and thus this feedback loop might function at the tissue level. Moreover, this genetic cascade explains the autoregulatory nature of *Mesp2* expression. We have noticed in our previous work that expression of *Mesp2* itself (*Mesp2-lacZ*) is strongly expanded in the absence of the Mesp2 function (Fig. 1K,L,N,O). This expansion of *Mesp2-lacZ* expression is coincident with the expansion of *Dll1* expression [see figure 5 by Takahashi et al. (Takahashi et al., 2000)]. In addition, this expanded expression of *Mesp2-lacZ* is lost in the Dll1/Mesp2 double-null embryo, indicating that it is dependent on Dll1 (Fig. 1M,P). The auto- and reciprocal regulations of *Dll1* and *Mesp2* are illustrated in Fig. 1R. Thus, Dll1-Notch signaling results in both activation and suppression of *Dll1* expression.

Mesp2 affects rostrocaudal properties more directly than Dll1

Next, we analyzed interactions between *Dll1* and *Mesp2* in regulation of rostral and caudal half marker genes, to address which gene more directly specifies rostrocaudal properties. In the *Mesp2*-null embryo, expression of the rostral marker genes *Cer1* and *Notch2* is severely decreased, while expression of the caudal marker genes *Dll1* and *Uncx4.1* is strongly expanded, suggesting that Mesp2 suppresses caudal and activates rostral properties. However, expression of both rostral and caudal marker genes is severely decreased in the Dll1-null embryo (del Barco Barrantes et al., 1999), suggesting that Dll1 might be involved in specifying both rostral and caudal characteristics. Expression of *Cer1* is usually observed as two stripes, finally localizing to the rostral half of nascent somites in the wild-type embryo (Fig. 2A). The stripe of *Cer1* expression is severely downregulated in both Dll1-null and Mesp2-null embryos, as well as in the Dll1/Mesp2 double-null embryo (Fig. 2B-D), suggesting that Dll1 and Mesp2 lie in the same cascade in regulating expression of rostral marker genes. Although *Dll1* expression is expanded in the absence of Mesp2, no *Cer1* induction is observed, suggesting that *Cer1* is not directly induced by Dll1 but by Mesp2.

We next observed the expression pattern of the caudal half marker gene, *Uncx4.1*. Normal stripes of *Uncx4.1* expression are completely lost in the Dll1-null embryo, indicating that *Dll1* lies upstream of *Uncx4.1* (Fig. 2E,F). In the Mesp2-null embryo, expression of both *Dll1* and *Uncx4.1* is strongly expanded, suggesting the involvement of Dll1 in the expansion of *Uncx4.1* expression (Fig. 2G). If only Dll1 specifies the caudal half property, as expected from our previous model, the lack of Mesp2 should not affect the loss of the caudal half property in the Dll1-null embryo. However, additional loss of *Mesp2* in the Dll1-null embryo results in the reappearance of *Uncx4.1* expression (Fig. 2H), indicating that *Uncx4.1* had been suppressed by Mesp2 in the Dll1-null embryo. *Mesp2* expression in the Dll1-null embryo is greatly reduced (Fig. 1H), but this trace amount of Mesp2 expression must be enough to suppress *Uncx4.1* expression. Therefore, even in the absence of Dll1, *Uncx4.1* is expressed in the somite region by loss of Mesp2 (Dll1/Mesp2 double-null embryo). However, the level of *Uncx4.1* expression is obviously higher in the Mesp2-null embryo than in the Dll1/Mesp2 double-null embryo,

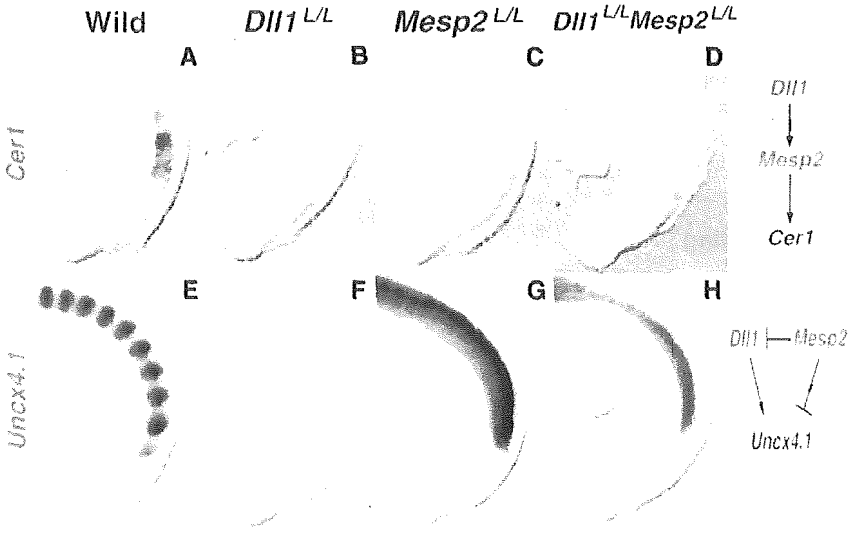

Fig. 2. Dll1 is required for normal expression of both rostral and caudal genes, and Mesp2 suppresses the caudal half property in both Dll1-dependent and Dll1-independent manners. Expression of *Cer1* is usually observed as two or three stripes, finally localizing to the rostral half of nascent somite in the wild-type embryo (A). *Cer1* expression is almost lost in both Dll1-null and Mesp2-null embryos (B,C), as well as the Dll1/Mesp2 double-null embryo (D). Normal stripes of *Uncx4.1* expression, localizing to the caudal half of each somite (E), are completely lost in the Dll1-null embryo (F). In Mesp2-null embryos, expression of both *Dll1* (Fig. 1) and *Uncx4.1* is strongly expanded (G). However, the additional loss of *Mesp2* in the Dll1-null embryo results in an expanded pattern of *Uncx4.1* expression (H). Genetic cascades are also shown.

showing that Dll1 can induce *Uncx4.1* in the absence of Mesp2. This indicates that *Uncx4.1* is induced by Dll1, and is also suppressed by Mesp2 independently of Dll1. We conclude, therefore, that Mesp2 suppresses the caudal half property in both Dll1-dependent and Dll1-independent manners. Thus, the Dll1-null phenotype is not a default state, and Mesp2 function is required for the manifestation of the Dll1-null phenotype.

Dll3 and Mesp2 are required for normal expression of each other

Dll3 is the other Notch ligand expressed in the PSM, and its expression finally localizes to the rostral half of each somite (Dunwoodie et al., 1997). The *Pudgy* mutant (*Dll3*$^{pu/pu}$, Dll3-null) embryo exhibits expression of both rostral and caudal half marker genes, but the patterns are spatially disorganized (Kusumi et al., 1998). Thus, we cannot readily conclude from the pudgy phenotype alone whether the Dll3-Notch signal results in activation or suppression of *Dll1*. To explore the roles of Dll3 in formation of the rostrocaudal polarity of somites, we first examined the mutual regulation of *Dll3* and *Mesp2*. *Pudgy* is a frame-shift mutation caused by a four-nucleotide deletion (Kusumi et al., 1998), allowing us to analyze expression of *Dll3* transcript in the *Dll3*$^{pu/pu}$ embryo. Comparison between wild and *Dll3*$^{pu/pu}$ embryos has revealed that the rostral stripes of *Dll3* expression are lost in the absence of functional Dll3 (Fig. 3A,B) (Kusumi et al., 1998), indicating that Dll3 is required for formation of the stripe pattern of its own expression. A relatively clear boundary in the expression level was observed between the PSM and somite region in the *Dll3*$^{pu/pu}$ embryo. The level of *Mesp2* expression is significantly decreased in the *Dll3*$^{pu/pu}$ embryo, suggesting that Dll3 upregulates expression of *Mesp2* (Fig. 3C,D). Finally, in the Mesp2-null embryo, instead of stripe formation, a weak diffuse *Dll3* expression is expanded rostrally (Fig. 3E,F). The above observations show that Dll3 induces expression of *Dll3* itself and *Mesp2*, while Mesp2 suppresses expression of *Dll3*. Thus, the regulatory interactions between *Dll3* and *Mesp2* appear similar to those of *Dll1* and *Mesp2*. However, the expansion of *Dll3* expression in the absence of Mesp2 is also observed in the Dll3/Mesp2 double-null embryo, indicating that it does not depend on Dll3 (Fig. 3G-J). This situation is different from that for *Dll1* and *Mesp2* (Fig. 1Q). Thus, the regulatory relationship between *Dll3* and *Mesp2* is similar to but different from that between *Dll1* and *Mesp2*. Taken together, both *Dll3* and *Mesp2* are necessary for their mutual normal expression. This indicates that stripe pattern of *Dll3*, as well as that of *Dll1*, is formed by involvement of Mesp2, and not simply by the molecular clock oscillating in the posterior PSM.

Mesp2 genetically lies downstream of *Dll3* regarding rostrocaudal polarity

Next, we analyzed genetic interaction between *Dll3* and *Mesp2* to elucidate their hierarchy during formation of the rostrocaudal polarity. (For the rostral genes, see supplemental Fig. S1 at http://dev.biologists.org/supplemental/.) The rostrocaudal patterning defects in the *Dll3*$^{pu/pu}$ embryo (Kusumi et al., 1998) and in the Mesp2-null embryo (Takahashi et al., 2000) have been previously reported, but we compared four genotypes (wild-type, *Dll3*$^{pu/pu}$, Mesp2 null, Dll3/Mesp2 double null) among our littermates for the precise evaluation of the double-null embryos. In the wild-type embryo, expression of *Dll1* is localized in the caudal half of each somite, with strong expression in the caudal PSM (Fig. 4A). However, only weak, blurred and randomized expression, instead of normal definite stripes, is seen in the somite region of the *Dll3*$^{pu/pu}$ embryo (Fig. 4B). In the Mesp2-null embryo, strong expression of *Dll1* is expanded rostrally (Fig. 4C). The Dll3/Mesp2 double-null embryo exhibited expansion of strong *Dll1* expression, indistinguishable from that in the Mesp2-null embryo (Fig. 4D). *Uncx4.1* expression is also localized in the caudal half of formed somites in the wild-type embryo (Fig. 4E). The *Dll3*$^{pu/pu}$ embryo exhibits a blurred and disorganized (salt-and-pepper) pattern of *Uncx4.1* expression (Fig. 4F), while the Mesp2-null embryo exhibits strong expansion of

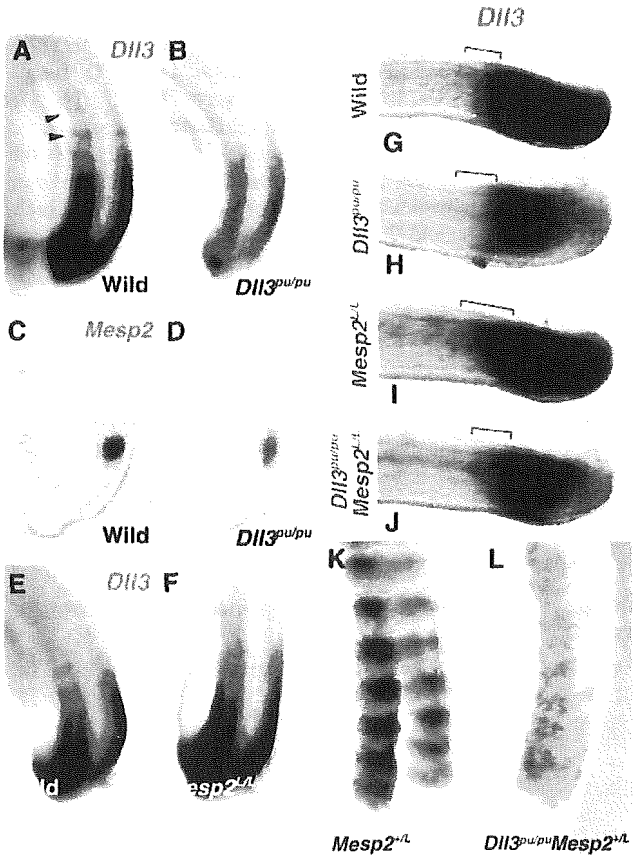

Fig. 3. Dll3 and Mesp2 are required for normal expression of each other. In the wild-type embryo at 9.5 dpc, expression of *Dll3* is finally localized to the rostral half of each somite (A). The *Dll3* stripe (arrowhead in A) is missing in the *Dll3*$^{pu/pu}$ embryo (B). The level of *Mesp2* expression is significantly decreased in the *Dll3*$^{pu/pu}$ embryo (C,D). In the Mesp2-null embryo, a weak diffuse *Dll3* expression is expanded rostrally (E,F). (G-J) Expansion of *Dll3* expression in the Mesp2-null embryo does not require Dll3. At 11.5 dpc, in the *Dll3*$^{pu/pu}$ embryo, the *Dll3* stripe is missing and the expression is not expanded rostrally (G,H). Expansion of *Dll3* expression in the Mesp2-null embryo is not largely affected by the loss of Dll3 (I,J). (K,L) Dll3 is required for localization of *Mesp2* expression into the rostral half of somites. In the wild type, β-gal activity for *Mesp2-lacZ* is localized in the rostral half of somites (K). A randomized salt-and-pepper pattern is observed in the *Dll3*$^{pu/pu}$ embryo (L).

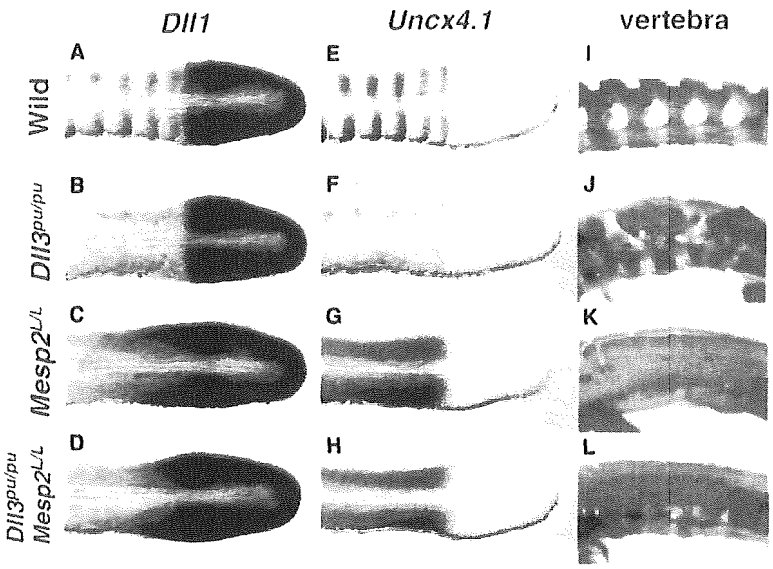

Fig. 4. Genetically, *Mesp2* lies downstream of *Dll3* regarding the rostrocaudal polarity. Expression of the caudal genes *Dll1* (A-D), *Uncx4.1* (E-H) and the morphology of the lumbar vertebrae (I-L) are examined in the Dll3/Mesp2 intercross. Genotypes are indicated on the left. The *Dll3/Mesp2* double-null embryo exhibits phenotypes indistinguishable from those of the Mesp2-null embryo. Details are stated in the text. For the rostral genes, see Fig. S1 at http://dev.biologists.org/supplemental/.

Uncx4.1 expression (Fig. 4G). As with *Dll1*, the Dll3/Mesp2 double-null embryo shows an *Uncx4.1* expression pattern indistinguishable from that in the Mesp2-null embryo (Fig. 4H). Finally, we examined the skeletal morphology of the lumbar vertebra. The pedicles and the laminae of the neural arches are arranged metamerically in the wild-type vertebral column (Fig. 4I). The *Dll3*$^{pu/pu}$ vertebrae show disorganized skeletal elements, partially fused to each other (Fig. 4J). The pedicles and the laminae are almost completely fused in the Mesp2-null fetus (Fig. 4K). The Dll3/Mesp2 double-null vertebrae exhibit almost completely fused neural arches (Fig. 4L). These observations indicate that *Mesp2* genetically lies downstream of *Dll3*, and that the salt-and-pepper pattern of *Uncx4.1* expression in the Dll3-null embryo requires the function of Mesp2. In other words, Mesp2 functions independent of Dll3 to suppress the caudal genes, *Dll1* and *Uncx4.1*, while Dll3 function is mediated by Mesp2. To know the function of Dll3 on Mesp2-mediated suppression on caudal genes, we further investigate their relationship. As Mesp2 is active in the *Dll3*$^{pu/pu}$ embryo with the salt-and-pepper pattern of *Dll1* and *Uncx4.1* expression, and localization of Mesp2 is crucial for rostrocaudal patterning, we examined the localization of *Mesp2-lacZ* expression in the *Dll3*$^{pu/pu}$ background by X-gal staining (Fig. 3K,L). Although expression of *Mesp2* mRNA at the rostral PSM simply seems moderately reduced and blurred (Fig. 3D), β-galactosidase activity in the somite region exhibited a salt-and-pepper pattern, instead of normal rostrally-localizing stripes (Fig. 3K,L). Thus, one major function of Dll3 is to localize expression of *Mesp2*.

Dll1-Notch signaling consists of both Psen1-dependent and Psen1-independent pathways

We have previously demonstrated that Mesp2-null and Psen1-null embryos exhibit contrastive rostrocaudal polarity of somites (Takahashi et al., 2000). To define whether Psen1 is involved in the Dll1-Notch or Dll3-Notch signaling pathway, we examined genetic interactions between *Psen1* and *Dll1* or *Dll3*. Examination of *Uncx4.1* expression in Dll1/Psen1 intercrosses proved that *Uncx4.1* expression is lost in both Dll1 and Psen1-null embryos, as well as in the Dll1/Psen1 double-null embryo (Fig. 5A-D). Therefore the induction of the caudal marker *Uncx4.1* is probably mediated by the Psen1-dependent Dll1-Notch signals. By contrast, the stripe expression of the rostral marker *Cer1* is only slightly decreased and expanded in the Psen1-null embryo, whereas it is almost lost in the Dll1-null embryo (Fig. 5E-G). The expanded *Cer1* expression in the Psen1-null embryo is lost by the additional loss of *Dll1* (the Dll1/Psen1 double-null embryo, Fig. 5H), implying that it is induced by the Psen1-independent Dll1-Notch signaling. The same result was obtained with the other rostral marker genes, *Epha4* and *Hoxd1* (data not shown). As Dll1 is required for the normal level of *Mesp2* expression that induces the expression of rostral genes, the requirement of Dll1 is likely to reflect the induction of *Mesp2*. Actually, expression of *Mesp2* is correlated with those of *Cer1* and *Epha4* (Fig. 5I-L). As *Mesp2* expression is moderately reduced in the Psen1-null embryo and is severely down-regulated in the Dll1/Psen1 double-null embryo, induction of *Mesp2* is likely to be mediated by both Psen1-dependent and Psen1-independent Notch signaling. These observations suggest that at least Psen1-independent Dll1-Notch signaling induces *Mesp2* and thereby rostral genes such as *Cer1*. However, both Dll1 and Dll3 contribute to the Psen1-dependent signals. Therefore, we analyzed the interaction of *Dll3* and *Psen1*.

Dll3-Notch signals are also both Psen1-dependent and Psen1-independent

The expression level of *Mesp2* was moderately decreased in the Dll3-null, Psen1-null and Dll3/Psen1 double-null embryos, and they were comparable among the three genotypes, suggesting that *Mesp2* expression is partly dependent on Psen1-dependent Dll3-Notch signaling (Fig. 5M-P). However, the remaining *Mesp2* expression observed in Dll3/Psen1 double-null embryo is dependent on neither Dll3 nor Psen1, confirming that this expression of *Mesp2* is induced via Psen1-independent Dll1-Notch signaling as already suggested (Fig. 5).

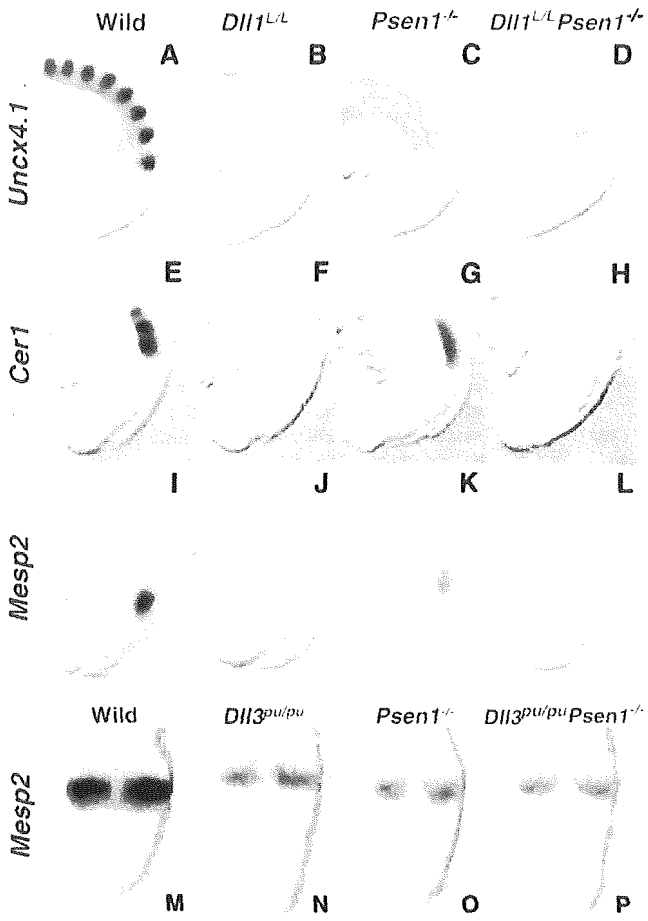

Fig. 5. Dll1-Notch signaling consists of both Psen1-dependent and Psen1-independent pathways. Normal *Uncx4.1* expression (A) is lost in both Dll1 (B) and Psen1-null (C) embryos, as well as in Dll1/Psen1 double-null embryo (D). The stripe expression of the rostral marker *Cer1* (E) is almost lost in the Dll1-null embryo (F), whereas it is expanded in the Psen1-null embryo (G). This expanded expression is lost by the additional loss of *Dll1* (the Dll1/Psen1 double-null embryo, H). Likewise, *Mesp2* expression (I) is almost lost in the Dll1-null embryo (J), moderately reduced in the Psen1-null embryo (K) and is almost lost in the Dll1/Psen1-double null embryo (L). (M-P) *Mesp2* expression is partly dependent on Psen1-dependent Dll3-Notch signaling. When compared with the wild type (M), expression levels of Mesp2 are decreased in the Dll3-null (N), Psen1-null (O) and Dll3/Psen1 double-null (P) embryos, and they are comparable among the three genotypes.

The expression patterns of caudal marker genes were correlated with the morphology of the vertebrae (Fig. 6). In the *Psen1*-null embryo ($Dll3^{+/+}Psen1^{-/-}$), stripes of *Dll1* and *Uncx4.1* expression were completely lost, and the pedicles of the neural arches were missing (Fig. 6C,H,M) (Takahashi et al., 2000). Although blurred *Dll1* expression was not detected, weak disorganized *Uncx4.1* expression was observed in the Dll3/Psen1 double-null embryo ($Dll3^{pu/pu}Psen1^{-/-}$, Fig. 6D,I). This level of *Uncx4.1* expression was lower than that in the $Dll3^{pu/pu}$, but distinguishable from that in the $Dll3^{+/+}Psen1^{-/-}$. This suggests that Dll3 can suppress expression of *Dll1* and *Uncx4.1* in the absence of Psen1, and Psen1 can mediate the Dll1-Notch signal to induce expression of *Dll1* and *Uncx4.1* in the absence of Dll3. These are further confirmed by the analyses of skeletal phenotypes. The vertebrae of $Dll3^{pu/pu}Psen1^{-/-}$ exhibited an intermediate morphology between $Dll3^{pu/pu}$ and $Dll3^{+/+}Psen1^{-/-}$ vertebrae. Whereas the $Dll3^{pu/pu}$ vertebrae had a considerable amount of disorganized skeletal elements in the position of the pedicles (Fig. 6L), the amount of disorganized skeletal elements was smaller in the vertebrae of $Dll3^{pu/pu}Psen1^{-/-}$ (Fig. 6N). Thus, the phenotype of $Dll3^{pu/pu}Psen1^{-/-}$ embryos differs from the phenotypes of both $Dll3^{pu/pu}$ and $Dll3^{+/+}Psen1^{-/-}$ embryos.

Dll3 and *Psen1* can counteract each other

Surprisingly, the loss of one copy of *Dll3* in the Psen1-null embryo restored the stripe pattern of gene expression. The $Dll3^{+/pu}Psen1^{-/-}$ embryo exhibited faint stripes of *Dll1* and *Uncx4.1* expression (Fig. 6E,J), and a small amount of skeletal elements at the position of the pedicles, although not regularly arranged (Fig. 6O). This indicates that Psen1-mediated Dll1-Notch signals and Dll3-Notch signals counteract each other in regulating *Dll1* and *Uncx4.1* expression, and establishing rostrocaudal polarity. In other words, the stripe pattern of gene expression is formed on a balance of two counteracting signals. Taken together, Dll3 and Psen1 can function independently, and have at least in some cases, opposite functions. This is also demonstrated in the morphology of the proximal ribs (see supplemental Fig. S2 at http://dev.biologists.org/supplemental/).

DISCUSSION

Dll1, Dll3 and Psen1 differentially regulate the rostrocaudal polarity of somites

Our results on involvement of Dll1, Dll3, Mesp2 and Psen1 in establishment of the rostrocaudal polarity are summarized in Fig. 7A. The present findings clarify the ligands for Notch signaling pathways in our previous model. *Dll1* is activated by the Psen1-dependent Dll1-Notch signaling pathway and suppressed by the Psen1-independent Dll3-Notch pathway. However, this suppressive Dll3 pathway is not sufficiently active in the absence of Mesp2. Mesp2 plays a major role in suppression of the caudal genes, including *Uncx4.1*, more directly than Dll1 or Dll3. In our previous model, (1) rostral localization of *Mesp2* expression is given a priori and (2) Dll1 exclusively specifies caudal half properties. However, the present scheme shows that both Dll1 and Dll3 influence the expression of *Mesp2*. Thus, these genes constitute a complex network, and interactions among these genes result in the simultaneous localization of *Dll1*, *Dll3* and *Mesp2*. In addition, Dll1-Notch signal is required for both rostral and caudal properties, as it induces *Dll1* itself and *Mesp2*. In contrast to Dll1, Dll3 upregulates *Mesp2* and suppresses *Dll1* and *Uncx4.1*, resulting in the suppression of caudal half properties. This is the first report specifying the functional differences of Dll1 and Dll3 in somite patterning. It should be noted, however, that the scheme in Fig. 7A does not immediately represent signaling cascades within single cells, but instead represents results from complex intercellular interactions among mesodermal cells in the rostral PSM.

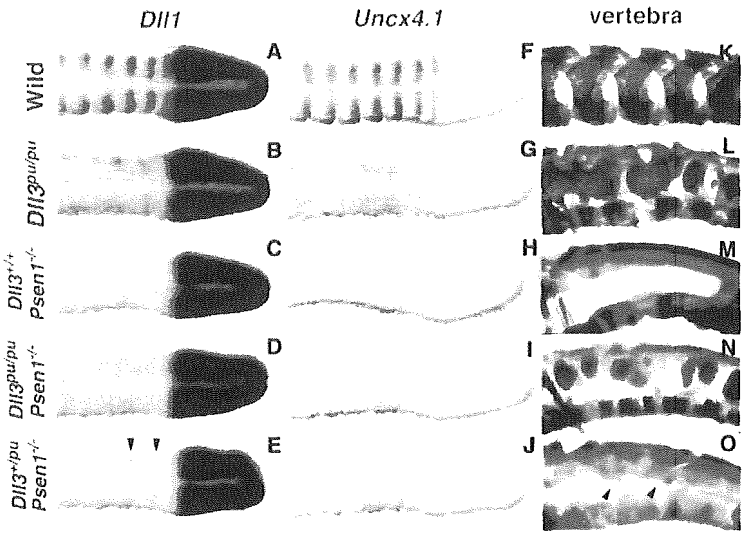

Fig. 6. Dll3 and Psen1 can act independently of each other in regulation of the caudal genes. The stripe pattern of *Dll1* and *Uncx4.1* is correlated with the skeletal morphology of the vertebrae (A,F,K). In the *Dll3*$^{pu/pu}$ embryo, the blurred and randomized expression of *Dll1* and *Uncx4.1* results in disorganized skeletal elements (B,G,L). In the Psen1-null embryo (*Dll3*$^{+/+}$*Psen1*$^{-/-}$), stripes of *Dll1* and *Uncx4.1* expression, and the pedicles were completely lost (C,H,M). Weak disorganized expression of *Uncx4.1* was observed in the Dll3/Psen1 double-null embryo (*Dll3*$^{pu/pu}$*Psen1*$^{-/-}$; D,I). The vertebrae of *Dll3*$^{pu/pu}$*Psen1*$^{-/-}$ exhibited an intermediate morphology between Dll3-null and Psen1-null vertebrae (N). Surprisingly, the *Dll3*$^{+/pu}$*Psen1*$^{-/-}$ embryo exhibited faint stripes of *Dll1* (E, arrowheads) and *Uncx4.1* (J), and a small amount of skeletal elements (O, arrowheads).

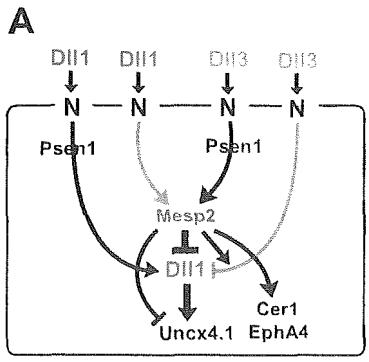

Fig. 7. (A) Summary of putative signaling cascades in the anterior PSM. The Psen1-independent pathways are shown with green arrows. Dll1-Notch signaling results in induction of both *Dll1* itself and *Mesp2*. The positive feedback of *Dll1* is mediated by the Psen1-dependent signal. Induction of *Mesp2* is mediated via Psen1-independent Dll1-Notch signaling and Psen1-dependent Dll3-Notch signaling. In contrast to Dll1, Dll3 has roles in upregulation of *Mesp2* and suppression of *Dll1* and *Uncx4.1*. (B) Integration of stripe pattern by Dll3 function. For simplification, anterior PSM cells of four-cell width are illustrated. Pink cells represent the dominance of the Mesp2 function, and blue cells the dominance of the Dll1 function. Genes and arrows are shown only between two representative cells for simplicity. The green arrows show the Psen1-independent pathways and broken lines show inactive states. Even in the absence of Dll3, Dll1-Notch signaling and Mesp2 are still active (left). Reciprocal Dll1-Notch signaling between two neighboring cells results in induction of *Dll1* in both cells. Meanwhile, reciprocal Dll1-Notch signaling also induces expression of *Mesp2*, which suppresses expression of *Dll1* cell-autonomously in both cells. When *Dll1* is downregulated, Mesp2 is also reduced by the lack of the juxtacrine Dll1 signal. Thus, the positive and negative feedback loops of *Dll1* and *Mesp2* produce uneven spatial patterns of Dll1 and Mesp2, but fail to form integrated stripe patterns in the absence of Dll3. Although the precise mechanism is unknown, participation of Dll3 results in synchronization of Dll1-dominant and Mesp2-dominant cells by suppressing *Dll1* expression in cooperation with Mesp2 (right). After segregation, Dll3 and Mesp2 continue to suppress *Dll1* and *Uncx4.1* expression in the rostral half, while Dll1 induces expression of *Dll1* itself and *Uncx4.1* via Psen1-dependent pathway in the caudal half. In the caudal half, induction of *Mesp2* expression via Psen1-independent pathway is inactive.

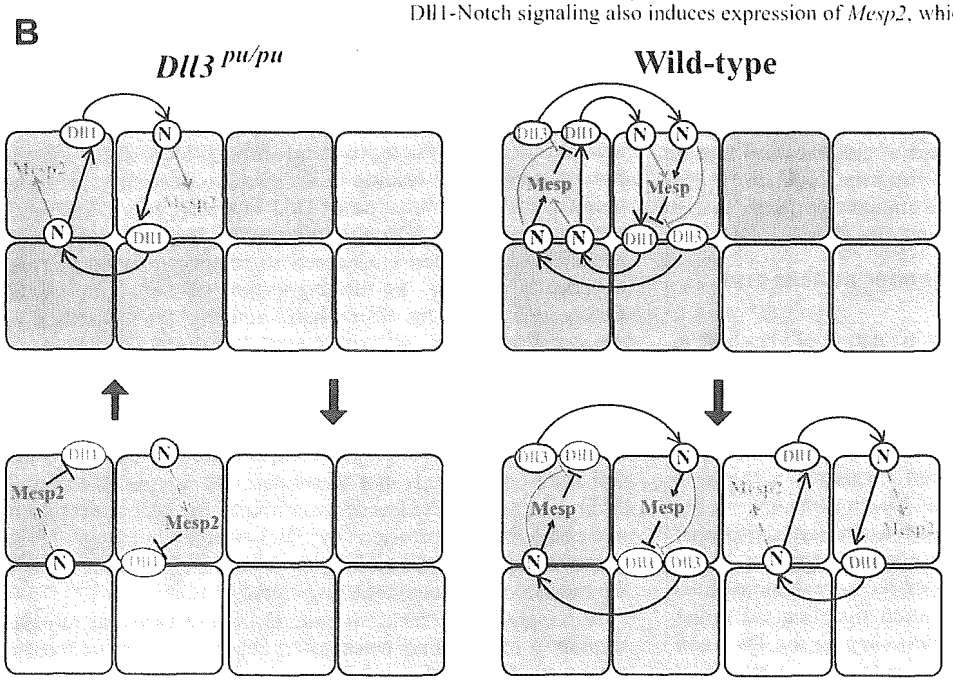

Stripe formation in the anterior PSM and oscillation in the posterior PSM

Expression of some genes considered to reflect the molecular clock, such as chick *hairy1*, oscillates as a 'traveling wave' in the posterior PSM, stabilizes at the anterior PSM and finally forms a half-a-somite stripe retained in somites (Palmeirim et al., 1997). Therefore, the rostrocaudal patterning, i.e. formation of half-a-somite stripe pattern of gene expression, has been regarded as a result of stabilization of oscillating expression in the posterior PSM. However, our analysis of the mutual regulation of *Dll1*, *Dll3* and *Mesp2* has demonstrated that none of the half-a-somite stripe patterns of *Dll1*, *Dll3* and *Mesp2-lacZ* are formed in the absence of Mesp2 function (Figs 1, 3). In particular, expression of *Mesp2-lacZ* is strongly expanded in the Mesp2-null embryo, implying that expression of *Mesp2* does not simply conform to the stripe prepattern formed by the molecular clock. This is in contrast to the stripes of *Uncx4.1-lacZ* in the absence of Uncx4.1 function (Mansouri et al., 2000), where expression of *Uncx4.1-lacZ* faithfully reflects the stripe prepattern formed in advance. At present, there is no evidence of the half-a-somite stripe prepattern upstream of *Mesp2*.

There is another example that the oscillation in the posterior PSM seems to be separated from the stripe formation. Holley et al. (Holley et al., 2002) have reported the interesting observation that in zebrafish embryos injected with her1-MO, a normal stripe of *deltaC* expression is formed in the anterior PSM, in the absence of oscillation of *deltaC* or *her1* in the posterior PSM. In this case, the *deltaC* stripe at the anterior PSM is not a result of simple stabilization of oscillating expression in the posterior PSM, but is likely to be formed by another mechanism. This stripe formation also appears to be mediated by Notch signaling, because the additional loss of DeltaD function disrupts stripe formation. In addition, injection of her1/her7 double-MO completely abolishes stripe formation (Oates and Ho, 2002). Holley et al. suggested that Notch signaling acts in oscillation of cyclic gene expression in the posterior PSM as well as in stripe formation (refinement of the stripe) at the anterior PSM. We propose that the narrowing stripe is formed at the anterior PSM, by the positive and negative feedback loops among *Dll1*, *Dll3* and *Mesp2*. These feedback loops may constitute a kind of cellular oscillator in the anterior PSM, which is distinct from the oscillator in the posterior PSM (Fig. 7B). This process may be normally linked with the oscillation process in the posterior PSM.

Interpretation of the salt-and-pepper pattern and possible functions of Dll3

The remarkably randomized and chaotic nature of vertebrae in the pudgy mouse has long been a mystery for geneticists. The salt-and-pepper pattern of gene expression in the Dll3-null mouse embryo is similar to that in zebrafish mutants *aei*, *des* and *bea*. Jiang et al. (Jiang et al., 2000) attributed this salt-and-pepper pattern to a desynchronized oscillator activity in individual cells, and concluded that Notch signaling is not essential for the oscillator activity itself, as the salt-and-pepper pattern is regarded as a result of a complete lack of Notch function in zebrafish mutants. However, we have demonstrated by genetic analysis that both Dll1-Notch signaling via Psen1 (Fig. 6) and Mesp2 (Fig. 4) are functioning in the Dll3-null embryo (Fig. 7B). We propose a model for rostrocaudal patterning, where the positive and negative feedback loops of *Dll1* and *Mesp2* and their integration by Dll3 are essential (Fig. 7B). Even in the absence of Dll3, *Dll1* and *Mesp2* are still expressed at considerable levels, and interactions among adjacent cells can result in two different states. The Dll1-Notch signal activates expression of *Dll1* in neighboring cells, thus causing upregulation of *Dll1* in a group of cells. Subsequently, the reciprocal Dll1-Notch signal also induces *Mesp2* expression, which suppresses *Dll1* expression so that *Dll1* is downregulated in the cell population. When *Dll1* is downregulated, *Mesp2* levels are also reduced by the lack of the juxtacrine Dll1 signal. Thus, the cells can 'oscillate' between the two states in the absence of Dll3. With some impact of initial stochastic activation, these interactions may produce and maintain uneven salt-and-pepper patterns of gene expression. In the wild-type embryo, involvement of Dll3 leads to synchronization of Dll1-dominant and Mesp2-dominant cells, and thus integration of the stripe pattern. As Mesp2 functions to activate rostral properties and suppresses caudal properties, the Mesp2-dominant domain is referred to as the presumptive rostral domain. The current model is a further development of our previous model (Takahashi et al., 2000). In our previous paper we showed that the stripe of *Dll1* expression is not a remainder of strong expression in the posterior PSM, but is newly induced via Psen1-dependent Notch signaling. That is, all the cells spanning the future one somite region undergo suppression by Mesp2, and the *Dll1* stripe is formed after or simultaneously with this suppression. We now interpret this process to be a result of the integration of cellular oscillation at the individual cellular level.

What then is the synchronizing function of Dll3 at the cellular level? The salt-and-pepper pattern of *Dll1* and *Uncx4.1* expression in the $Dll3^{pu/pu}$ embryo has somewhat confused the issue of whether the Dll3-Notch signal activates or suppresses *Dll1* expression. As the level of blurred and mislocalized *Dll1* expression in the $Dll3^{pu/pu}$ embryo is lower than that of definite *Dll1* stripes in the wild-type embryo, one might consider that Dll3 function is required for activation of *Dll1*. However, strong expansion of *Dll1* expression is evident in the Dll3/Mesp2 double-null embryo, as well as in the Mesp2-null embryo, indicating that Dll3 is not necessary for the auto-activation of *Dll1* via a positive feedback loop. Although the precise mechanism leading to the synchronization is yet to be defined, the likely function of Dll3 is to suppress Dll1-Notch signaling, probably in cooperation with Mesp2. This function seems feasible when considered in relation to their normal expression patterns, as the expression of *Dll3* and *Mesp2* finally localizes to the rostral half. Actually, the restoration of the stripe pattern of *Dll1* and *Uncx4.1* in the $Dll3^{+/pu}Psen1^{-/-}$ embryo implies that Dll3-Notch signaling can counteract Psen1-dependent Dll1-Notch signaling. This phenomenon also suggests that the stripe pattern is formed by a balance of two opposing signals. Probably, the requirement of Psen1 for the activation of *Dll1* is not absolute, and in the Psen1-null embryo, a severely reduced, weak ability for *Dll1* activation is overcome by suppression by Dll3-Notch signaling. Thus, reduction of the amount of the Dll3-Notch signal may restore the balance of the counteracting signals.

In the posterior PSM, Dll1 and Dll3 have essential roles in formation of traveling waves of cyclic genes such as lunatic fringe and *Hes1* (del Barco Barrantes et al., 1999; Jouve et al.,

2000; Dunwoodie et al., 2002). Therefore, we cannot exclude the possibility that Dll1 and Dll3 influence the rostrocaudal patterning through their effects on the molecular clock in the posterior PSM. Analysis of the possible linkage between stripe formation at the anterior PSM and the oscillation process in the posterior PSM is of special importance for understanding the roles of Notch signaling in somitogenesis.

We thank Mariko Ikumi, Seiko Shinzawa and Eriko Ikeno for general technical assistance. We also thank Yasushi Hiromi and Sadao Yasugi for critical reading of the manuscript. This work was supported by Grants-in-Aid for Science Research on Priority Areas (B) and the Organized Research Combination System of the Ministry of Education, Culture, Sports, Science and Technology, Japan.

REFERENCES

Bessho, Y., Sakata, R., Komatsu, S., Shiota, K., Yamada, S. and Kageyama, R. (2001). Dynamic expression and essential functions of *Hes7* in somite segmentation. *Genes Dev.* **15**, 2642-2647.

Bettenhausen, B., Hrabe de Angelis, M., Simon, D., Guénet, J.-L. and Gossler, A. (1995). Transient and restricted expression during mouse embryogenesis of Dll1, a murine gene closely related to *Drosophila* Delta. *Development* **121**, 2407-2418.

Conlon, R. A., Reaume, A. G. and Rossant, J. (1995). *Notch1* is required for the coordinate segmentation of somites. *Development* **121**, 1533-1545.

del Barco Barrantes, I., Elia, A. J., Wünsch, K., de Angelis, M. H., Mak, T. W., Rossant, J., Conlon, R. A., Gossler, A. and de la Pompa, J. L. (1999). Interaction between Notch signaling and Lunatic fringe during somite boundary formation in the mouse. *Curr. Biol.* **9**, 470-480.

De Strooper, B., Annaert, W., Cupers, P., Saftig, P., Craessaerts, K., Mumm, J. S., Schroeter, E. H., Schrijvers, V., Wolfe, M. S., Ray, W. J., Goate, A. and Kopan, R. (1999). A presenilin-1-dependent γ-secretase-like protease mediates release of Notch intracellular domain. *Nature* **398**, 518-522.

Dornseifer, P., Takke, C. and Campos-Ortega, J. A. (1997). Overexpression of a zebrafish homologue of the *Drosophila* neurogenic gene *Delta* perturbs differentiation of primary neurons and somite development. *Mech. Dev.* **63**, 159-171.

Dunwoodie, S. L., Henrique, D., Harrison, S. M. and Beddington, R. S. P. (1997). Mouse Dll3: a novel divergent Delta gene which may complement the function of other Delta homologues during early pattern formation in the mouse embryo. *Development* **124**, 3065-3076.

Dunwoodie, S. L., Clements, M., Sparrow, D. B., Sa, X., Conlon, R. A. and Beddington, R. S. P. (2002). Axial skeletal defects caused by mutation in the spondylocostal dysplasia/pudgy gene Dll3 are associated with disruption of the segmentation clock within the presomitic mesoderm. *Development* **129**, 1795-1806.

Evrard, Y. A., Lun, Y., Aulehla, A., Gan, L. and Johnson, R. L. (1998). *lunatic fringe* is an essential mediator of somite segmentation and patterning. *Nature* **394**, 377-381.

Forsberg, H., Crozet, F. and Brown, N. A. (1998). Waves of mouse Lunatic fringe expression, in four-hour cycles at two-hour intervals, precede somite boundary formation. *Curr. Biol.* **8**, 1027-1030.

Haddon, C., Smithers, L., Schneider-Maunoury, S., Coche, T., Henrique, D. and Lewis, J. (1998). Multiple *delta* genes and lateral inhibition in zebrafish primary neurogenesis. *Development* **125**, 359-370.

Holley, S. A., Geisler, R. and Nüsslein-Volhard, C. (2000). Control of her1 expression during zebrafish somitogenesis by a delta-dependent oscillator and an independent wave-front activity. *Genes Dev.* **14**, 1678-1690.

Holley, S. A., Julich, D., Rauch, G.-J., Geisler, R. and Nüsslein-Volhard, C. (2002). *her1* and the *notch* pathway function within the oscillator mechanism that regulates zebrafish somitogenesis. *Development* **129**, 1175-1183.

Hrabe de Angelis, M., McIntyre, J., II and Gossler, A. (1997). Maintenance of somite borders in mice requires the *Delta* homologue *Dll1*. *Nature* **386**, 717-721.

Jiang, Y. J., Aerne, B. L., Smithers, L., Haddon, C., Ish-Horowicz, D. and Lewis, J. (2000). Notch signaling and the synchronization of the somite segmentation clock. *Nature* **408**, 475-479.

Jouve, C., Palmeirim, I., Henrique, D., Beckers, J., Gossler, A., Ish-Horowicz, D. and Pourquié, O. (2000). Notch signaling is required for cyclic expression of the hairy-like gene HES1 in the presomitic mesoderm. *Development* **127**, 1421-1429.

Koizumi, K., Nakajima, M., Yuasa, S., Saga, Y., Sakai, T., Kuriyama, T., Shirasawa, T. and Koseki, H. (2001). The role of presenilin 1 during somite segmentation. *Development* **128**, 1391-1402.

Kusumi, K., Sun, E. S., Kerrebrock, A. W., Bronson, R. T., Chi, D. C., Bulotsky, M. S., Spencer, J. B., Birren, B. W., Frankel, W. N. and Lander, E. S. (1998). The mouse *pudgy* mutation disrupts *Delta* homologue *Dll3* and initiation of early somite boundaries. *Nat. Genet.* **19**, 274-278.

Mansouri, A., Voss, A. K., Thomas, T., Yokota, Y. and Gruss, P. (2000). Uncx4.1 is required for the formation of the pedicles and proximal ribs and acts upstream of Pax9. *Development* **127**, 2251-2258.

McGrew, M. J., Dale, J. K., Fraboulet, S. and Pourquié, O. (1998). The lunatic fringe gene is a target of the molecular clock linked to somite segmentation in avian embryos. *Curr. Biol.* **8**, 979-982.

Nomura-Kitabayashi, A., Takahashi, Y., Kitajima, S., Inoue, T., Takeda, H. and Saga, Y. (2002). Hypomorphic *Mesp* allele distinguishes establishment of rostro-caudal polarity and segment border formation in somitogenesis. *Development* **129**, 2473-2481.

Oates, A. C. and Ho, R. K. (2002). *Hairy/E(spl)-related (Her)* genes are central components of the segmentation oscillator and display redundancy with the Delta/Notch signaling pathway in the formation of anterior segmental boundaries in the zebrafish. *Development* **129**, 2929-2946.

Oka, C., Nakano, T., Wakeham, A., de la Pompa, J. L., Mori, C., Sakai, T., Okazaki, S., Kawaichi, M., Shiota, K., Mak. T. W. and Honjo, T. (1995). Disruption of the mouse *RBP-Jk* gene results in early embryonic death. *Development* **121**, 3291-3301.

Palmeirim, I., Henrique, D., Ish-Horowicz, D. and Pourquié, O. (1997). Avian *hairy* gene expression identifies a molecular clock linked to vertebrate segmentation and somitogenesis. *Cell* **91**, 639-648.

Saga, Y., Hata, N., Koseki, H. and Taketo, M. M. (1997). *Mesp2*: a novel mouse gene expressed in the presegmented mesoderm and essential for segmentation initiation. *Genes Dev.* **11**, 1827-1839.

Saga, Y. and Takeda, H. (2001). The making of the somite: molecular events in vertebrate segmentation. *Nat. Rev. Genet.* **2**, 835-845.

Struhl, G. and Greenwald, I. (1999). Presenilin is required for activity and nuclear access of Notch in *Drosophila*. *Nature* **398**, 522-525.

Takahashi, Y., Koizumi, K., Takagi, A., Kitajima, S., Inoue, T., Koseki, H. and Saga, Y. (2000). Mesp2 initiates somite segmentation through the Notch signalling pathway. *Nat. Genet.* **25**, 390-396.

Takke, C. and Campos-Ortega, J. A. (1999). Her1, a zebrafish pair-rule gene, acts downstream of notch signaling to control somite development. *Development* **126**, 3005-3014.

Wong, P. C., Zheng, H., Chen, H., Becher, M. W., Sirinathsinghji, D. J. S., Trumbauer, M. E., Chen, H. Y., Price, D. L., van der Ploeg, L. H. T. and Sisodia, S. S. (1997). Presenilin 1 is required for *Notch1* and *Dll1* expression in the paraxial mesoderm. *Nature* **387**, 288-292.

Ye, Y., Lukinova, N. and Fortini, M. E. (1999). Neurogenic phenotypes and altered Notch processing in *Drosophila Presenilin* mutants. *Nature* **398**, 525-529.

Zhang, N. and Gridley, T. (1998). Defects in somite formation in *lunatic fringe*-deficient mice. *Nature* **394**, 374-377.

ARTICLE IN PRESS

Available online at www.sciencedirect.com

SCIENCE DIRECT®

Life Sciences

ELSEVIER

Life Sciences xx (2005) xxx – xxx

www.elsevier.com/locate/lifescie

Effect of the difference in vehicles on gene expression in the rat liver—analysis of the control data in the Toxicogenomics Project Database

Kayoko Takashima [a], Yumiko Mizukawa [a,c], Katsumi Morishita [a], Manabu Okuyama [a], Toshihiko Kasahara [a], Naoki Toritsuka [a], Toshikazu Miyagishima [a,b], Taku Nagao [a], Tetsuro Urushidani [a,b,c,*]

[a] *Toxicogenomics Project, National Institute of Health Sciences, 1-18-1 Kamiyoga, Setagaya-Ku, Tokyo, 158-8501, Japan*

[b] *Present address of Toxicogenomics Project, National Institute of Biomedical Innovation, 7-6-8, Saito-Asagi, Ibaraki, Osaka, 567-0085, Japan*

[c] *Department of Pathophysiology, Faculty of Pharmaceutical Sciences, Doshisha Women's College of Liberal Arts, Kodo, Kyotanabe, Kyoto 610-0395, Japan*

Received 30 July 2005; accepted 1 November 2005

Abstract

The Toxicogenomics Project is a 5-year collaborative project by the Japanese government and pharmaceutical companies in 2002. Its aim is to construct a large-scale toxicology database of 150 compounds orally administered to rats. The test consists of a single administration test (3, 6, 9 and 24 h) and a repeated administration test (3, 7, 14 and 28 days), and the conventional toxicology data together with the gene expression data in liver as analyzed by using Affymetrix GeneChip are being accumulated. In the project, either methylcellulose or corn oil is employed as vehicle. We examined whether the vehicle itself affects the analysis of gene expression and found that corn oil alone affected the food consumption and biochemical parameters mainly related to lipid metabolism, and this accompanied typical changes in the gene expression. Most of the genes modulated by corn oil were related to cholesterol or fatty acid metabolism (e.g., CYP7A1, CYP8B1, 3-hydroxy-3-methylglutaryl-Coenzyme A reductase, squalene epoxidase, angiopoietin-like protein 4, fatty acid synthase, fatty acid binding proteins), suggesting that the response was physiologic to the oil intake. Many of the lipid-related genes showed circadian rhythm within a day, but the expression pattern of general clock genes (e.g., period 2, arylhydrocarbon nuclear receptor translocator-like, D site albumin promoter binding protein) were unaffected by corn oil, suggesting that the effects are specific for lipid metabolism. These results would be useful for usage of the database especially when drugs with different vehicle control are compared.

Keywords: Toxicogenomics; Vehicle control; Methylcellulose; Corn oil; Lipid metabolism; Rat; Liver

Introduction

The Toxicogenomics Project is a 5-year collaborative project by the National Institute of Health Sciences (NIHS) and 17 pharmaceutical companies in Japan which started in 2002 (Urushidani and Nagao, 2005). In April 2005, some rearrangements were made and now the project is conducted by NIHS, the National Institute of Biomedical Innovation, and 16 pharmaceutical companies. Its aim is to construct a large-scale toxicology database of transcriptome for prediction of toxicity of new chemical entities in the early stage of drug development. About 150 chemicals, mainly medicinal compounds, have been selected, and the following are examined for each. The in vivo test using rat consists of a single administration test (3, 6, 9 and 24 h with 4 dose levels including vehicle control) as well as a repeated administration test (3, 7, 14 and 28 days with 4 dose levels including vehicle control), and the data of body weight, general symptoms, histopathological examination of liver and kidney, and blood biochemistry are obtained from each animal. The gene expression in liver (and kidney in some cases) is comprehensively analyzed by using Affymetrix GeneChip. An in vitro test using rat and human hepatocytes is also carried out to accomplish the bridging between the species. By April 2005, more than 100 chemicals, covering wide medication categories, have been finished or are ongoing.

* Corresponding author. Department of Pathophysiology, Faculty of Pharmaceutical Sciences, Doshisha Women's College of Liberal Arts, Kodo, Kyotanabe, Kyoto 610-0395, Japan. Tel.: +81 0774 65 8689.

E-mail address: turushid@dwc.doshisha.ac.jp (T. Urushidani).

0024-3205/$ - see front matter © 2005 Published by Elsevier Inc.
doi:10.1016/j.lfs.2005.11.010

Along with the effects of the chemicals, a vast amount of control data is being accumulated.

The main purpose of the project is to predict toxicity in the early stage of drug development. The potential usefulness of microarray data for the estimation of toxicity of drugs makes it possible for this technology to be used in the late stage of development, i.e., application in the field of regulatory science. In this case, however, more strict and precise validation is needed in order to assure the reliability of the data. It is well known that a difference in the platform considerably effects a variation in the microarray data (Waring et al., 2004) and this is quite difficult to overcome. In our project, either methylcellulose or corn oil is employed as vehicle, according to the dispensability of the drug. It is quite possible that the difference in the vehicle control affects the analysis, as observed by multiple comparison of drug effects. In traditional toxicological study, comparison of the drug is exclusively made against its vehicle control. However, in the transcriptome database, it is usually necessary to make a comparison among various drugs by clustering or discriminant analysis. The history of this field is not old enough for collecting appropriate data regarding this issue. Our database enables us to make various comparisons among different vehicles, protocols, facilities, chip versions, etc. In this present report, we focus on the influence of vehicles on the control parameters including the gene expression profile in the rat liver as a basic study for future analysis.

Materials and methods

Animal treatment

Male Sprague-Dawley rats were purchased from Charles River Japan Inc., (Kanagawa, Japan) at 5-weeks of age. After a 7-day quarantine and acclimatization period, the animals were divided into groups of 5 animals using a computerized stratified random grouping method based on the body weight for each age. The animals were individually housed in stainless-steel cages in a room that was lighted for 12 h (7:00–19:00) daily, ventilated with an air-exchange rate of 15 times per hour, and maintained at 21–25 °C with a relative humidity of 40–70%. Each animal was allowed free access to water and pellet food (CRF-1, sterilized by radiation, Oriental Yeast Co., Japan).

According to the protocol in our project, rats in each group were orally administered with various drugs suspended or dissolved either in 0.5% methylcellulose solution or corn oil according to their dispersibility. Each drug had 4 different dose levels, including the vehicle control alone, which was exclusively analyzed in the present study. Drug treatment was performed between 9:00 and 11:30 a.m. For single-dose experiments, rats were sacrificed at 3, 6, 9, and 24 h after dosing. For repeated dose experiments, the animals were treated for 3, 7, 14 or 28 days, and they were sacrificed 24 h after the last dosing. Body weights were recorded every day while food consumption was recorded every 4 days during repeated dosing. Blood samples were collected upon sacrifice in tubes containing heparin lithium (blood biochemistry), EDTA-2K (hematology), or 1/9 vol of 3.8% citric acid (coagulation), and the following items were examined: hematology: the numbers of red blood cells, reticulocytes, white blood cells, eosinophils, monocytes, platelets, neutrophils, basophils, and lymphocytes, hemoglobin, mean red blood cell volume, mean hemoglobin contents, and mean hemoglobin concentration (Advia 120, Bayer); blood coagulation: prothorombin time, active partial prothrombin time, and fibrinogen (Sysmex CA-5000, Sysmex); and blood biochemistry: alkaline phosphatase, total cholesterol, triglyceride, phospholipid, total and direct bilirubin, glucose, blood urea nitrogen, creatinine, Na, K, Ca, Cl, inorganic phosphate, total protein, albumin, globulin/albumin ratio, aspartate aminoptansferase, alanine aminotransferase, lactate dehydrogenase, and γ-glutamyltranspeptidase, which were determined by an auto-analyzer (Hitachi 7080).

When the analysis was performed (April 2005), 65 compounds had been completed in 4 different contract research organizations. In order to eliminate the variations due to the difference in the facility, we selected a laboratory (Japan Bioassay Center, Kanagawa, Japan) where at least 7 experiments for each vehicle were completed. As 10 experiments were done with methylcellulose as the vehicle there, the latest 3 of them were excluded from the present analysis to match the numbers. Therefore, each time point consists of 35 (5 rats for 7 experiments) animals.

The experimental protocols were reviewed and approved by the Ethics Review Committee for Animal Experimentation of National Institute of Health Sciences.

Microarray analysis

After collecting the blood, the animals were euthanized by exsanguination from the abdominal aorta under ether anesthesia. An aliquot of the sample (about 30 mg) for RNA analysis was obtained from the left lateral lobe of the liver in each animal immediately after sacrifice, kept in RNA later® (Ambion, Austin, TX, USA) overnight at 4 °C, and then frozen to send to the facility in the National Institute of Health Sciences.

Total RNA was isolated using RNeasy kit by Bio Robot 3000 (Qiagen, Valencia, CA, USA). Homogenization was conducted by Mill Mixer (Qiagen) and zirconium beads. Purity of the RNA was checked by gel electrophoresis confirming the 260/280 nm ratio was between 2.0 and 2.2.

Microarray analysis was conducted on 3 out of 5 samples for each group by using GeneChip® RAE230A probe arrays (Affymetrix, Santa Clara, CA, USA), containing 15923 probe sets. The procedure was conducted basically according to the manufacturer's instructions using Superscript Choice System (Invitrogen, Carlsbad, CA, USA) and T7-$(dT)_{24}$-oligonucleotide primer (Affymetrix) for cDNA synthesis, cDNA Cleanup Module (Affymetrix) for purification, and BioArray High yield RNA Transcript Labeling Kit (Enzo Diagnostics, Farmingdale, NY, USA) for synthesis of biotin-labeled cRNA. Ten micrograms of fragmented cRNA was hybridized to a RAE230A probe array for 18 h at 45 °C at 60 rpm, after which the array was washed and stained by streptavidin-phycoerythrin using

Fluidics Station 400 (Affymetrix) and scanned by Gene Array Scanner (Affymetrix).

In the middle of the project (2004), Affymetrix released ver. 2.0 GeneChip and we switched from RAE230A to 230.2. Two out of seven experiments were performed using the new chips, and they were excluded from the present analysis in order to maintain consistency. Therefore, each time point consisted of 15 measures (3 rats for 5 experiments) in the case of gene expression analysis.

The digital image files were processed by Affymetrix Microarray Suite version 5.0 and the intensities were normalized for each chip by setting the mean intensity to 500 (per chip normalization). The results of the DNA microarray analysis are available upon request (e-mail to turushid@dwc.doshisha.ac.jp).

Statistical analysis

For conventional toxicological parameters, it is common that many unimportant changes with statistical significance are observed because of the large numbers of measurements. In the present study, more than 40 parameters were measured for 8 time points (3, 6, 9, 24 h for single and 3, 7, 14, 28 days for repeated administration). For comparison between methylcellulose and corn oil, we applied Student's t-test with Bonferroni's adjustment for each parameter, i.e., p value was multiplied by 8 and $p<0.01$ was considered to be statistically significant.

For gene expression data, it is problematic to use a standard t-test, because of too many comparisons, but it is also not good to use a too conservative adjustment, because of the small

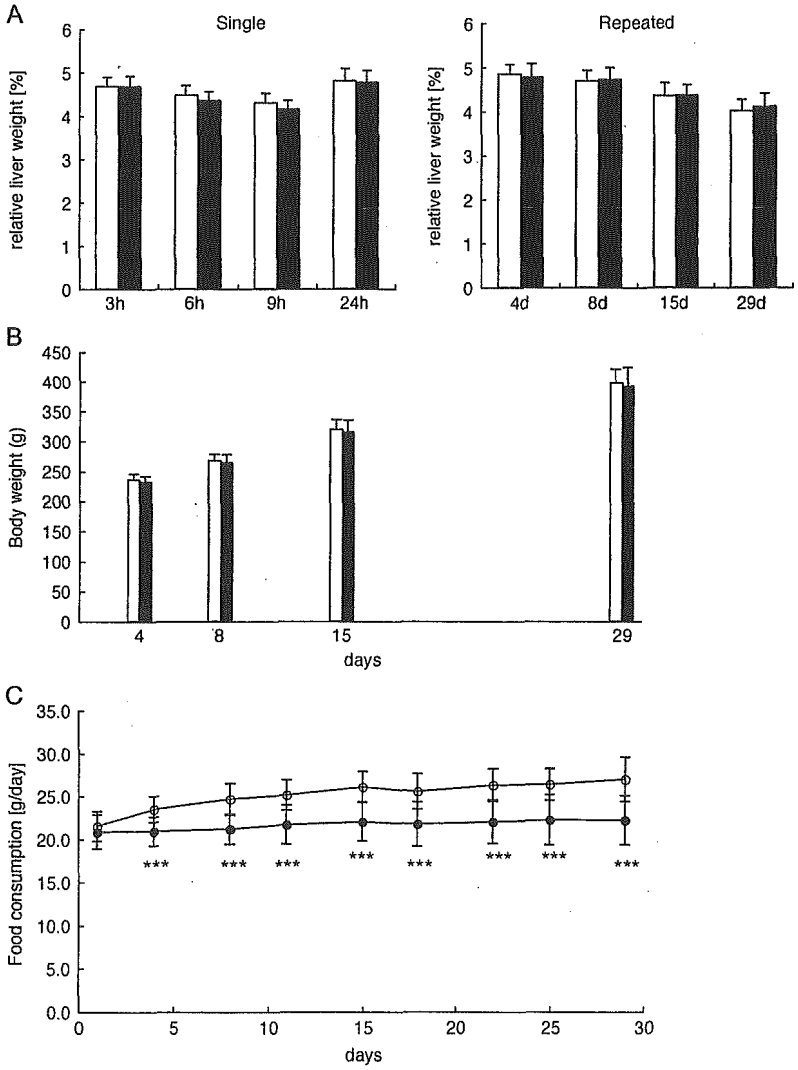

Fig. 1. Effects of different vehicles on relative liver weight, body weight, and food consumption of rats. Liver weight/body weight within 24 h after administration of vehicle and 24 h after the repeated administrations (for 3, 7, 14 and 28 days) of vehicle were measured at autopsy (A). Open and filled columns represent methylcellulose and corn oil, respectively. Body weight 24 h after the repeated administrations (for 3, 7, 14 and 28 days) of vehicle (B) and food consumption measured every 4 days and expressed as g/day (C) are plotted. Again, open and filled symbols represent methylcellulose and corn oil, respectively. Values are expressed as mean±SD of 35 rats each for each time point. Food consumption data were obtained from rats that received either vehicle for 28 days. ***Statistically significant between methylcellulose and corn oil by Student's t-test with Bonferroni's adjustment, at $p<0.001$.

numbers of samples compared with the numbers of genes. In the present study, we considered that the β-error should be small, since our purpose was to pick up the possible vehicle effects on gene expression. Before comparison, the genes that showed less than 20 of the expression value after per chip normalization in all the samples were excluded. Genes extracted were those showing at least 1.5 fold difference between two vehicles, with $p<0.01$ (uncorrected t-test).

Results

It is common that some statistically significant but unimportant differences are observed in toxicological tests where huge numbers of parameters are measured and compared. In the present analysis of the vehicle effect, there appeared to be some differences that could not be ignored. Fig. 1A depicts the relative weight of the liver (liver weight/body weight). As is widely known, this parameter showed a clear circadian rhythm, i.e., it decreases toward the evening (9 h after dosing) and goes back in the next morning (Fig. 1A, left). In the case of rats receiving corn oil, this parameter tended to be lower than that in methylcellulose group at 6 and 9 h after dosing ($p=0.03$ and $p=0.005$, respectively, by standard t-test, but $p=0.24$ and $p=0.04$, respectively, by Bonferroni's adjustment and not significant at $p<0.01$), whereas the values returned to the same level at 24 h after administration. There was no difference in this parameter in the repeated administration, suggesting that the tendency of the decrease in the liver weight by corn oil was not accumulated during repeated dosing (Fig. 1A, right). Fig. 1 shows the body weight change (B)

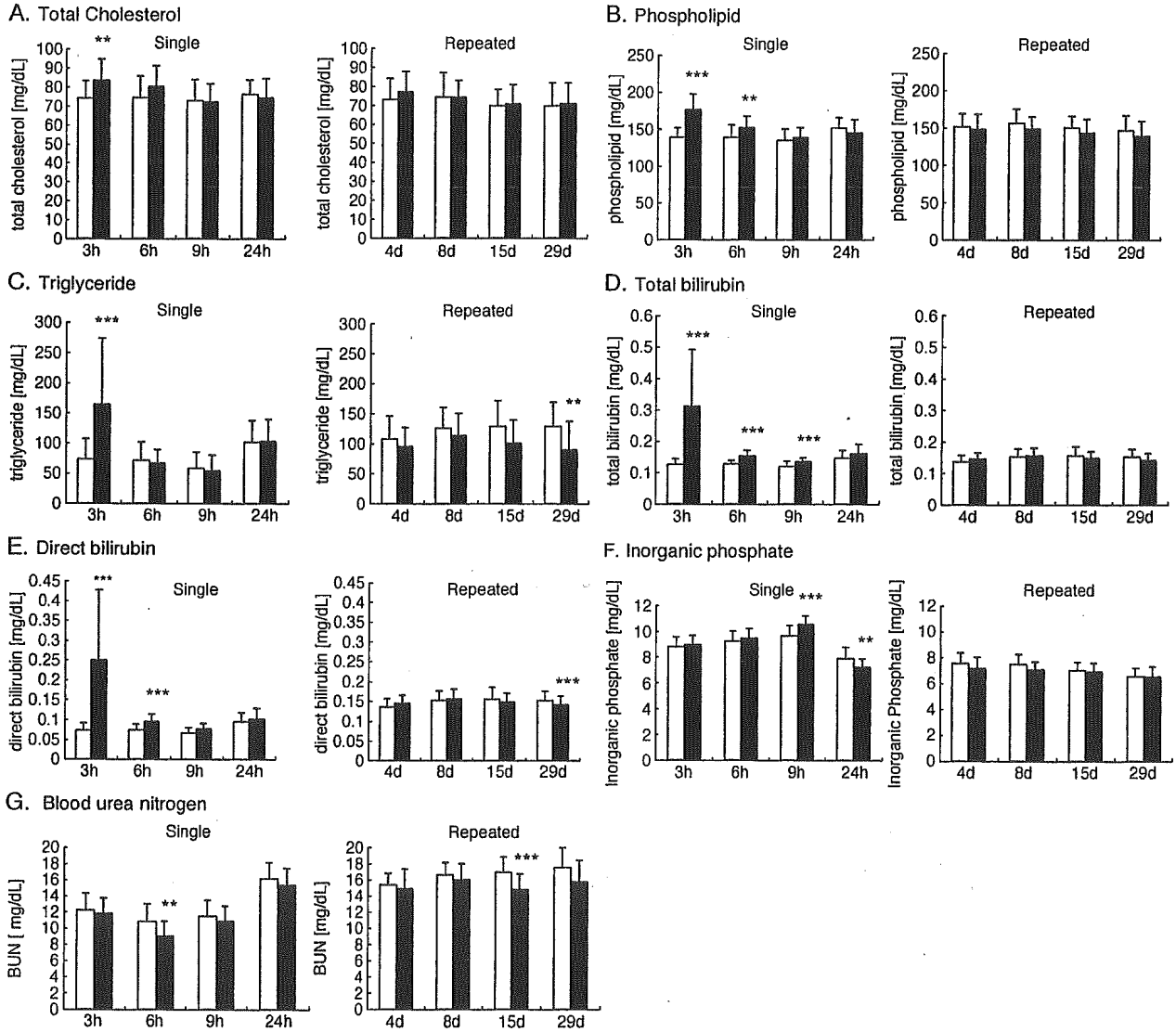

Fig. 2. Blood biochemical parameters in rats receiving methylcellulose or corn oil. Total cholesterol (A), triglyceride (B), phospholipid (C), total bilirubin (D) and direct bilirubin (E), inorganic phosphate (F), and blood urea nitrogen (G) showed a significant difference between methylcellulose (open columns) and corn oil (closed columns) among 36 parameters. Values are expressed as mean±SD of 35 rats for each time point. Statistically significant between methylcellulose and corn oil by Student's t-test with Bonferroni's adjustment, at $^{**}p<0.01$, $^{***}p<0.001$.